J. Fluid Mech. (1966), *vol.* 25, *part* 3, *pp.* 523–555
Printed in Great Britain

Free gravitational oscillations in rotating rectangular basins†

By DESIRAJU B. RAO
The University of Chicago‡

(Received 29 July 1965 and in revised form 30 November 1965)

The study of free oscillations of a homogeneous liquid under gravity in rotating rectangular basins of uniform depth is undertaken from both theoretical and experimental considerations.

The theoretical study is in the framework of the quasistatic equations. It is also assumed that the curvature of the free surface can be ignored. Numerical computations for the frequencies and modal structures were carried out for several of the slowest antisymmetric and symmetric modes in a square basin and in a rectangular basin of two-to-one dimension ratio, without any restriction on the angular speed of rotation of the basin. These computations are in agreement with a numerical value obtained many years ago by Taylor, and also with several values found by Corkan & Doodson. They exhibit the typical frequency-splitting associated with certain multiplets in the zero-rotation spectrum. Further, the theoretical calculations indicate that the slopes of the curves of frequency versus speed of rotation change sign for some of the modes in rectangular geometry. Such behaviour is not present in circular basins. Negative modes are found to be 'unstable' in the sense of Corkan & Doodson; that is, they are transformed into positive modes for sufficiently high rotation. Calculations were also made for the slowest longitudinal oscillations in highly elongated basins to demonstrate the decreasing importance of rotation on the frequencies of these modes.

Experimental work was carried out in a flat-bottomed square tank for the slowest positively and negatively propagating antisymmetric modes and the slowest positively propagating symmetric mode. Good agreement was found between theory and experiment.

PART 1. RESULTS OF THEORETICAL AND EXPERIMENTAL ANALYSIS

1. Introduction

The first solutions of the problem of free oscillations in rotating square and rectangular basins of uniform depth were derived by Rayleigh (1903, 1909). Rayleigh's treatment was restricted to the case where the rotation speed ω was small compared with the speed σ of the oscillation. Some of his results were in error,

† This paper is a condensed version of a Doctoral Dissertation (Rao 1965).

‡ Present affiliation: National Center for Atmospheric Research, Boulder, Colorado.

and were later corrected by Proudman (1933). Taylor (1922) gave the first complete solution (valid for any ω) for the free oscillations in a rectangular basin. Some of his conclusions were criticized by Jeffreys (1925), who pointed out that there was a double infinity of modes in the rotating case and that there might be modes travelling in both directions of the basin (with and against the rotation). Defant (1925) subsequently gave an approximate method of simplifying Taylor's analysis.

Lamb (1924) gave an approximation to the slowest speed by a different method. His result is

$$(\sigma^2 - \nu_1^2)(\sigma^2 - \nu_2^2) = 256\pi^{-4}\omega^2\sigma^2, \tag{1.1}$$

where ν_1 and ν_2 are the speeds of the slowest longitudinal and slowest transverse modes in the zero-rotation case. In the special case of a square $\nu_1 = \nu_2$ and (1.1) reduces to

$$\sigma - \nu_1 = \pm 8\pi^{-2}\omega. \tag{1.2}$$

This agrees with the result of Rayleigh (1903) as corrected by Proudman (1933). Lamb also showed that there are wave systems travelling in both directions round the basin. Goldsbrough (1931) solved the problem formally for any ω but approximated the results to small ω because of computational difficulties. In particular, he confirmed Lamb's results.

Corkan & Doodson (1952) treated the case of a square sea by direct numerical integration of the dynamic equations and obtained frequency values at a few rotation speeds for the slowest positively (in the same direction as rotation) and negatively (opposite the direction of rotation) propagating antisymmetric modes. (In an antisymmetric mode, the surface elevation at two points diagonally opposite with respect to the centre is the same in magnitude but opposite in sign; for a symmetric mode both the sign and the magnitude are the same.) They found that negative waves are 'unstable' in the sense that these waves are transformed into positive waves at high rotations.

The most recent investigation of the free oscillations in rotating rectangular basins is that of Van Dantzig & Lauwerier (1960). They obtained a solution valid for any ω but approximated the results to small values of ω. The explicit results obtained by them are

$$\sigma/\nu_1 = 1 \pm 0{\cdot}405(2\omega/\nu_1) + 0{\cdot}138(2\omega/\nu_1)^2 + \ldots \tag{1.3}$$

for a square. The minus sign refers to the slowest positive antisymmetric mode and the plus sign to the negative mode. This extends the approximation (1.2) of Lamb and Rayleigh by one more order in ω. For a 2×1 rectangle Van Dantzig & Lauwerier give an explicit result only for the lowest order in ω for the slowest positive antisymmetric mode

$$\sigma/\nu_1 = 1 - 0{\cdot}302(2\omega/\nu_1)^2, \tag{1.4}$$

which agrees with the result of Rayleigh (1909) as corrected by Proudman (1933), when specialized to the case of a 2×1 rectangle.

It is clear from this brief survey that the solution of the problem of free oscillations in rotating rectangular basins is far from being complete. The past studies, in addition to being restricted to small rotations, do not contain any

information on the behaviour of the higher modes and so the problem is re-examined here in detail. Computations were made for the frequencies and modal structures of several of the lowest symmetric and antisymmetric modes in a square and a 2×1 rectangle. The frequency results obtained from the present investigation for the slowest positive and negative antisymmetric modes in a square and the slowest positive antisymmetric mode in a 2×1 rectangle are presented in figure 1 along with the results from the past investigations. In this

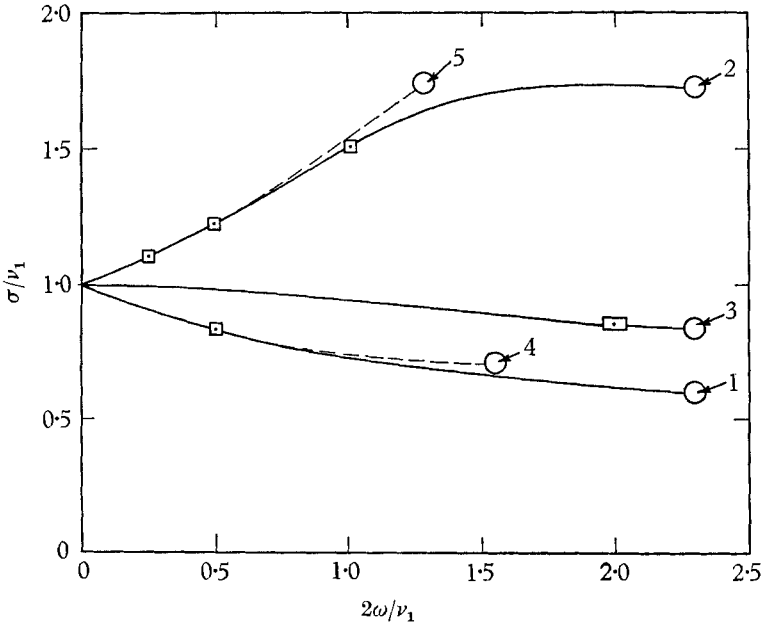

FIGURE 1. Frequency of oscillation (σ/ν_1) in square and rectangular basins of uniform depth, as a function of rotation speed ($2\omega/\nu_1$). The solid curves are the results of the present calculation: curves 1 and 2 correspond to the slowest positive and negative modes in a square and curve 3 to the slowest positive mode in a 2×1 rectangle. Also shown are Corkan & Doodson's (1952) results for a square (⊡) and Taylor's (1922) result for a 2×1 rectangle (⊡). Curves 4 and 5 show the results of Van Dantzig & Lauwerier's (1960) perturbation analysis for the slowest positive and negative modes in a square, valid through the second order of $2\omega/\nu_1$.

diagram the frequency of oscillation σ and the angular speed of rotation ω are non-dimensionalized by ν_1, the slowest zero-rotation frequency. It is seen that there is very good agreement between the present and the past results. Figure 1 also shows the incompleteness of the picture obtained from the past investigations alone. The complete results obtained from the present study are given in a later section.

Computations were made also for the lowest antisymmetric mode in 4×1 and 6×1 rectangles to show the decreasing importance of rotation on the frequencies of these modes. Also, experimental work was carried out in a square tank to determine the frequencies of the slowest positive and negative antisymmetric modes and the slowest positive symmetric mode, for comparison with the theory.

In the following we present a brief discussion of the method of solution and then the theoretical and experimental results. An outline of the mathematical analysis is given in part 2 and a summary is given in part 3. It is possible to read part 1 with little or no reference to part 2.

2. Method of analysis

The dynamical equations for free, quasistatic motion in an inviscid, homogeneous water mass are (Lamb 1932, § 207)

$$\partial \mathbf{V}/\partial t = -g\nabla\zeta + f[\mathbf{V}] \tag{2.1}$$

and

$$\partial\zeta/\partial t = -\nabla . H\mathbf{V}. \tag{2.2}$$

Here $\mathbf{V}$ is the horizontal velocity vector; ζ is the fluctuation of the free surface above its equilibrium level; g is the acceleration of gravity; $f \equiv 2\omega \sin\phi$, where ω is the angular speed of the earth's rotation and ϕ is the latitude; H is the equilibrium depth of the sea; ∇ denotes the horizontal gradient operator; t is the time; and $[\mathbf{V}]$ indicates a 90-degree clockwise rotation of $\mathbf{V}$ in the horizontal plane. For an enclosed sea, the boundary condition is

$$HV_n = 0, \tag{2.3}$$

where V_n is the component of $\mathbf{V}$ normal to the coast.

In the absence of rotation equations (2.1), (2.2), (2.3) permit standing modes of oscillation in a rectangular basin ($0 \leqslant x \leqslant a$; $0 \leqslant y \leqslant b$). For the case of uniform depth, the explicit solutions for the standing oscillations are:

$$\left.\begin{aligned} u &= a^{-1}k\pi \sin(a^{-1}k\pi x)\cos(b^{-1}l\pi y)\sin(\nu t+\Delta),\\ v &= b^{-1}l\pi \cos(a^{-1}k\pi x)\sin(b^{-1}l\pi y)\sin(\nu t+\Delta),\\ \text{and}\quad \zeta &= g^{-1}\nu \cos(a^{-1}k\pi x)\cos(b^{-1}l\pi y)\cos(\nu t+\Delta), \end{aligned}\right\} \tag{2.4}$$

where k and l are any two integers, Δ is an arbitrary phase angle, and the zero-rotation frequency ν is given by

$$\nu = \pi[(k^2/a^2 + l^2/b^2)gH]^{\frac{1}{2}}. \tag{2.5}$$

In (2.4), (u, v) are the components of $\mathbf{V}$ along the axes x, y in the horizontal plane. When the basin is rotating, it is not possible to write down simple solutions, such as (2.4), to describe the normal modes. In this case, the oscillations consist of wave systems travelling around the basin either in the positive or in the negative direction.

The principle used here in solving the normal-mode problem in the rotating case is based upon a method formulated by Proudman (1916), in which the velocity field $\mathbf{V}$ is partitioned uniquely into an irrotational part $\mathbf{V}^\phi$ and a rotational part $\mathbf{V}^\psi$, each of which is made to satisfy the boundary condition (2.3). Then expansions for $\mathbf{V}^\phi$, $\mathbf{V}^\psi$ are obtained in terms of certain orthogonal functions which also satisfy (2.3), and the expansion coefficients are determined so as to satisfy the dynamic equations (2.1) and (2.2).

In the following sections we present the results of the theoretical analysis. Before proceeding to do so, it is necessary to explain the notation that is used to

enumerate the modes. Consider the continuous transformation of a particular mode as the rotation of the basin goes to zero or, in other words, as $f \to 0$. If the frequency at $f = 0$ is a singlet, that is, if there is no other mode with the same frequency, then in this limit the modal configuration is that of a particular standing mode (2.4), and the original mode at $f \neq 0$ can be identified unambiguously as the '(k, l) mode', where (k, l) are the wave-numbers of the limiting zero-rotation standing mode. On the other hand, if the frequency at $f = 0$ is a multiplet of order $r > 1$ (meaning that there are r distinct standing modes having this frequency), then in this limit the modal configuration is a particular combination of r standing modes, each of the type (2.4). In order to associate the original mode at $f \neq 0$ with just one of these zero-rotation standing modes, we adopt the *ad hoc* procedure of perturbing the dimensions of the rectangle through a slight increase in the length of the side parallel to the x-axis. This has the effect of resolving the multiplet into r singlets, one of which is the zero-rotation limit of the (slightly perturbed) original mode.

In summary, with every mode at $f \neq 0$ we associate a certain zero-rotation standing mode, and we identify the mode at $f \neq 0$ by means of the wave-numbers of this standing mode (even though there may be little resemblance between the two).

3. Modal frequency

The results described in this and §§4 and 5 were obtained by means of a high-speed computer. (The method of computation is given in part 2.) The effect of rotation on the frequency was investigated specifically on twelve modes in a square and twelve modes in a 2×1 rectangle, namely those which at zero rotation are the slowest six antisymmetric and the slowest six symmetric modes. (The zero-rotation modes are antisymmetric if $k+l$ is odd and symmetric if $k+l$ is even in (2.4).) The modes in question are identified by the first column in tables 1 and 2 in accordance with the notation explained at the end of §2. The frequency values and rotation speeds in these tables are non-dimensionalized by the frequency ν_1 of the slowest zero-rotation oscillation, given by (2.5) with $(k, l) = (1, 0)$. The range of rotation considered is $0 \leqslant f/\nu_1 \leqslant 2{\cdot}25$ for antisymmetric modes (table 1) and $0 \leqslant f/\nu_1 \leqslant 2{\cdot}0$ for symmetric modes (table 2).

The contents of tables 1 and 2 are illustrated graphically in figure 2. This diagram exhibits the effect of rotation on all modes of the zero-rotation spectrum with frequencies in the range $\nu/\nu_1 < 4$ for the square and $\nu/\nu_1 < 5$ for the rectangle. The solid lines correspond to antisymmetric modes and the dashed lines to symmetric modes. The slowest mode of all is the antisymmetric mode (1, 0) which consists of one wave travelling in the positive direction of the basin; that is, in the same direction as that of rotation. As seen in figure 2, the (1, 0), (0, 1); (1, 2), (2, 1); (3, 0), (0, 3) modes in a square are examples of doublets in the zero-rotation frequency spectrum for antisymmetric modes. Other doublets can be seen from an examination of the figure. These multiplets in the zero-rotation spectrum are split into distinct frequencies on the introduction of rotation.

A comparison between the frequency behaviour of the slowest positively propagating antisymmetric mode (1, 0) in a square and the corresponding mode

in a circular cylinder, which is the (1, 1) mode in the (θ, r)-direction (for the latter, see Lamb 1932, §210) revealed the curious feature that the mode in the square has a frequency variation almost identical with that of the corresponding mode in a circle, within the accuracy of the present computations, in the rotation range

	f/ν_1								
Mode	0	0·25	0·50	1·00	1·25	1·50	1·75	2·00	2·25
					Square				
(1, 0)	1·0	0·907	0·831	0·723	0·686	0·657	0·635	0·617	0·602
(0, 1)	1·0	1·110	1·235	1·509	1·630	1·706	1·737	1·739	1·730
(1, 2)	2·236	2·173	2·119	2·058	2·074	2·151	2·290	2·468	2·666
(2, 1)	2·236	2·307	2·384	2·540	2·610	2·666	2·705	2·733	2·742
(3, 0)	3·0	2·997	3·012	3·092	3·157	3·241	3·347	3·471	3·612
(0, 3)	3·0	—	3·057	3·181	3·263	3·356	3·453	3·547	3·625
					Rectangle (2 × 1)				
(1, 0)	1·0	0·995	0·982	0·942	—	0·897	0·876	0·857	0·840
(0, 1)	2·0	2·015	2·058	2·201	—	2·336	2·364	2·369	2·361
(2, 1)	2·828	2·811	2·777	2·726	—	2·776	2·868	2·998	3·150
(3, 0)	3·0	3·025	3·083	3·235	—	3·402	3·483	3·554	3·615
(1, 2)	4·123	4·127	4·138	4·177	—	4·233	4·272	4·325	4·397
(4, 1)	4·472	4·472	4·472	4·489	—	4·556	4·609	4·670	4·735

TABLE 1. Frequencies σ/ν_1 of antisymmetric modes as a function of rotation speed f/ν_1

	f/ν_1					
Mode	0	0·25	0·50	1·00	1·50	2·00
				Square		
(1, 1)	1·414	1·405	1·380	1·313	1·253	1·206
(2, 0)	2·0	2·010	2·038	2·131	2·216	2·251
(0, 2)	2·0	2·022	2·084	2·293	2·577	2·902
(2, 2)	2·828	2·821	2·805	2·795	2·881	3·094
(1, 3)	3·162	3·166	3·176	3·213	3·254	3·297
(3, 1)	3·162	3·182	3·235	3·404	3·624	3·870
				Rectangle (2 × 1)		
(2, 0)	2·0	1·978	1·930	1·828	1·742	1·675
(1, 1)	2·236	2·266	2·338	2·528	2·732	2·896
(3, 1)	3·606	3·599	3·584	3·547	3·542	3·622
(0, 2)	4·0	4·006	4·022	4·084	4·170	4·257
(4, 0)	4·0	4·013	4·049	4·172	4·342	3·549
(2, 2)	4·472	4·478	4·497	4·570	4·693	4·865

TABLE 2. Frequencies σ/ν_1 of symmetric modes as a function of rotation speed f/ν_1

$f/\nu_1 < 2{\cdot}25$. Specifically, let $\sigma(1, 1)$ denote the frequency of the (1, 1) positive mode in a circular cylinder, and let $\nu(1, 1)$ denote the zero-rotation frequency of this mode. Then, if the values of $\sigma(1, 1)/\nu(1, 1)$ are plotted as a function of $f/\nu(1, 1)$, the points fall on the curve of the (1, 0) mode in a square (the lowest curve in the

left panel of figure 2) within the accuracy of computation. This correspondence appears to be coincidental since it is not found for the corresponding negative modes or for the higher modes.

There are other differences in the frequency behaviour between square or rectangular basins and circular basins. In the circular basin, restricting attention

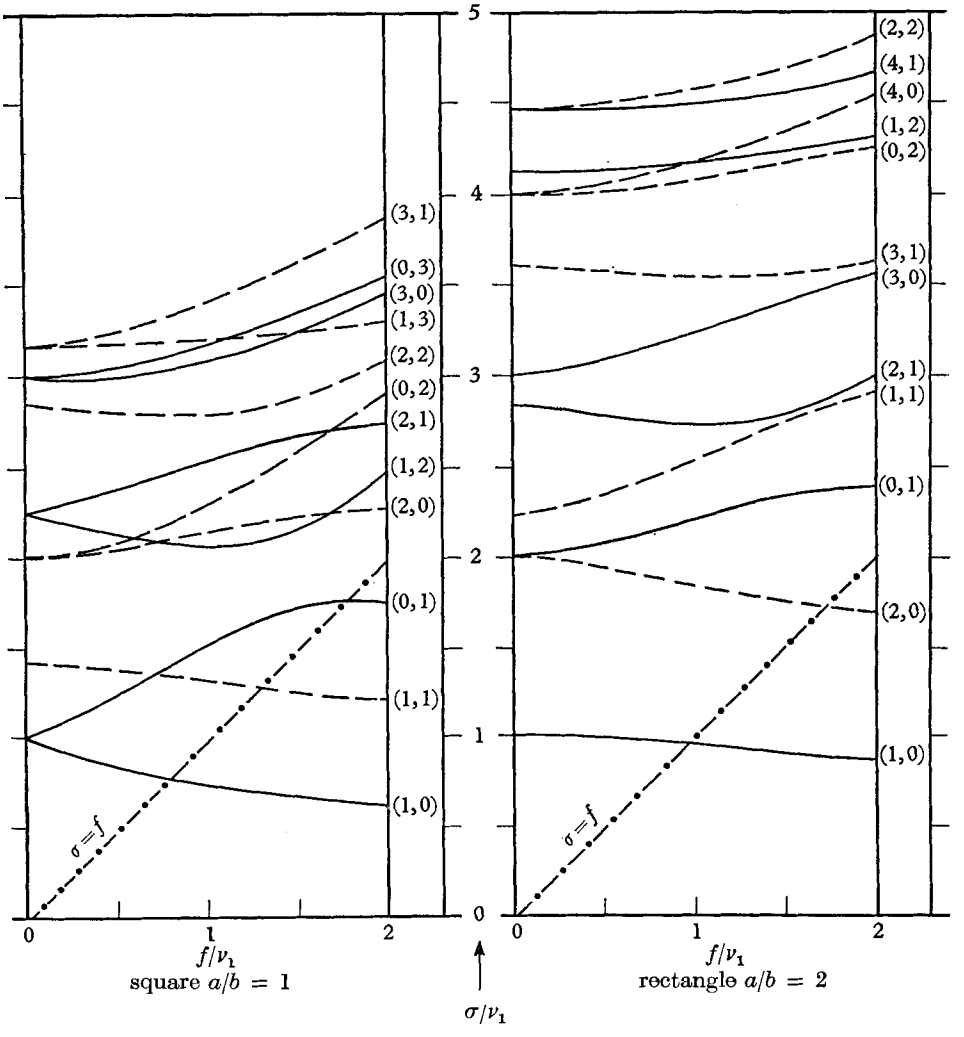

FIGURE 2. Frequency (σ/ν_1) *vs.* rotation speed (f/ν_1) for various modes in square and 2×1 rectangular basins.

to the azimuthal modes, each zero-rotation frequency is a doublet which splits into two distinct frequencies when $f \neq 0$. The mode with the lower frequency (absolute value) always propagates in the positive direction and the one with the higher frequency in the negative direction. Let integers i and j represent the wave-numbers in θ- and r-directions. Then in each set (a set being defined as the infinite number of pairs generated by all j for a fixed i) for the first positive wave

alone there is a value of f ($= f^*$, say) for which σ becomes equal to f. For $f < f^*$, $\sigma > f$ and, for $f > f^*$, $\sigma < f$. For all the other modes, $\sigma > f$ for all f. Moreover, for all modes σ/f decreases as f increases, and tends to the value 1 in the limit $f \to \infty$, except for the first positive mode of each set, for which $\sigma/f \to 0$; that is, each set of modes belonging to a given azimuthal wave-number has only one member with frequency in the range $0 < \sigma < f$. It is not obvious how to compare this feature of the circular geometry with what happens in rectangular geometry, but, if we consider a set here as corresponding to a fixed k and all l, an examination of figure 2 shows that for both square and rectangular basins it is possible to have $\sigma < f$ for more than one member of each set if f is greater than some critical value depending upon the mode.

Another very interesting feature of figure 2 is the non-monotonic behaviour of some of the frequency curves. (This does not happen in the case of a circular cylinder.) As an interesting consequence of this behaviour some of the modes have frequencies exactly equal to their zero-rotation frequencies at certain values of $f \neq 0$.

Taylor (1922) suggested that the roots of the period equation for the symmetric modes may fall between the roots for the antisymmetric modes. However, this depends on how one examines the roots. For example, even in the zero-rotation case if one considers the entire spectrum of frequencies obtained from (2.5), the roots of the antisymmetric and symmetric modes do not fall between each other. The same is true in the rotating case also, as can be seen from figure 2. On the other hand, if one considers the zero-rotation frequency spectrum obtained by taking a fixed k (or l) and letting l (or k) vary, then the roots of the antisymmetric modes fall between those of symmetric modes. Presumably this may happen in the rotating case also, in general. Within the range of the present computations it does happen so, as shown by figure 2.

Consider now the frequency behaviour in highly elongated basins. In table 3, the frequencies of the lowest longitudinal mode for $f/\nu_1 = 0$, 0·5, 1·0 for various elongations are given. It is evident from this table that the effect of rotation on the frequencies of the longitudinal oscillations becomes less important as the basin becomes more elongated. In the limit, these oscillations are transformed into Kelvin waves (Lamb 1932, §208). Hence, in treating the dynamics of a basin like Lake Erie for example ($a/b = 6$ and $f/\nu_1 = 0{\cdot}8$), ignoring the effect of the earth's rotation on the periods of oscillation is justifiable even though f is not small compared with the slowest oscillation speed. One can then make allowance for rotation effects on the motions by a Kelvin-wave hypothesis, as has been done by many investigators (for example, by Platzman & Rao 1964 in their study of the free periods of Lake Erie). That this gives reasonable results even from the point of view of modal structure will be shown later.

Consider now the purely transverse modes. In very elongated basins one would expect these modes to assume the form of waves with horizontal crests, the so-called Sverdrup waves, since the boundaries at $x = 0$ and a are too distant to affect significantly the main part of the motion. The frequency equation for these waves is (Proudman 1953, §132) $\sigma^2 = \nu^2 + f^2$, where ν is the zero-rotation frequency of the purely transverse modes, given by (2.5) with $k = 0$. In table 4

the exact frequency values of the lowest transverse mode for $f/\nu_1 = 0$, 0·5, 1·0, and for various elongations, are presented, together with the corresponding Sverdrup-wave frequencies. From an inspection of this table it is clear that the actual frequencies tend to those for a Sverdrup wave as the elongation ratio a/b increases.

	f/ν_1		
a/b	0	0·5	1·0
1	1·0	0·831	0·723
2	1·0	0·982	0·942
4	1·0	0·998	0·992
6	1·0	0·999	0·997

TABLE 3. Frequency σ/ν_1 of lowest longitudinal mode (1, 0) as a function of rotation speed f/ν_1 for various basin elongations a/b

	f/ν_1		
a/b	0	0·5	1·0
1	1·0 (1·0)	1·235 (1·118)	1·509 (1·414)
2	2·0 (2·0)	2·058 (2·062)	2·201 (2·236)
4	4·0 (4·0)	4·030 (4·031)	4·117 (4·123)
6	6·0 (6·0)	6·020 (6·021)	6·080 (6·083)

TABLE 4. Frequency σ/ν_1 of lowest transverse mode (0, 1) as a function of rotation speed f/ν_1 for various basin elongations. Sverdrup-wave frequency $(\nu^2+f^2)^{\frac{1}{2}}/\nu_1$ is given in parentheses

4. Modal structure

The perturbation height field ζ of any mode in the rotating case may be written as

$$\zeta(x,y,t) = A(x,y)\cos[\sigma t - \theta(x,y)].$$

Here $A(x,y)$ is the amplitude and $\theta(x,y)$ is the phase of high water at a point (x,y). The modal structures are presented here in terms of co-amplitude lines (contours of A) and co-tidal lines (contours of θ). The amplitude A is normalized to make the average value of A^2 over the basin equal to 100 in all cases. The co-tidal lines are drawn at intervals of one-twelfth period; that is, in θ-increments of 30 degrees through the range $0 \leqslant \theta < 360°$. The co-amplitude and co-tidal lines in figures 3–6 were drawn from values calculated at points equally spaced at intervals $\Delta x = 0{\cdot}025a = \Delta y$. This gives a resolution of 40×40 points for the square, and 40×20 points for the 2×1 rectangle. In all cases the rotation of the basin is positive (counter-clockwise) and each figure shows results for a square and for a 2×1 rectangle.

The slowest positively propagating mode (1, 0) is presented in figure 3, for rotation speed $f/\nu_1 = 2$. This mode, in both basins, consists of one wave travelling in the positive direction about an amphidromic point at the centre of the basin. (It may be noted, for comparison, that the co-tidal lines in the zero-rotation

case are straight lines and are fixed in space for all time.) The amplitude of oscillation is zero at the amphidromic point and increases outward; it reaches a maximum value at the corners. This structure of the mode remains essentially unchanged with increasing rotation. In the sequel we refer to an amphidromic point as positive or negative according as the associated wave system rotates in the positive (counter-clockwise) or negative (clockwise) sense.

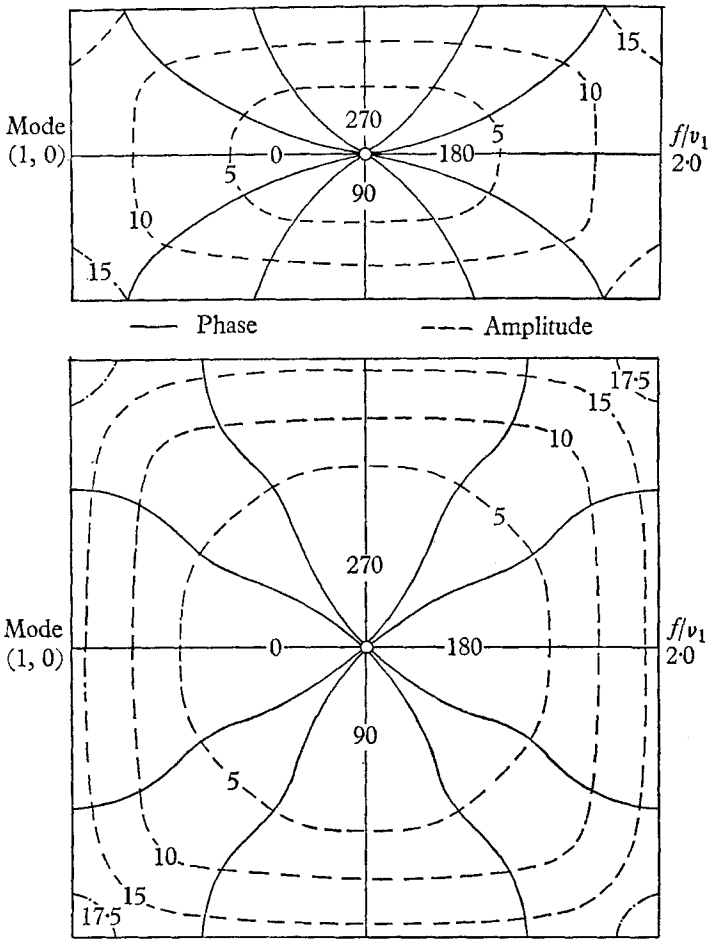

FIGURE 3. Structure of the slowest positive antisymmetric mode in a 2 × 1 rectangle and in a square. In this and the following diagrams, ○ represents a positive amphidromic system and ● a negative amphidromic system.

Figures 4(*a*), (*b*) and (*c*) represent the slowest negative mode at different values of f/ν_1. Taking first the case of a square, we see that for low rotation this mode consists of one wave travelling in a clockwise direction about an amphidromic point at the centre of the basin, as shown in figure 4(*a*). As the rotation increases, the structure of this mode changes, in marked contrast to the slowest positive mode. In particular, for a certain value of f/ν_1 (not precisely determined in this investigation, but in the range $1{\cdot}0 < f/\nu_1 < 1{\cdot}1$) a system of four positive amphidromic points enters the basin from the boundaries, as shown in figure 4(*b*).

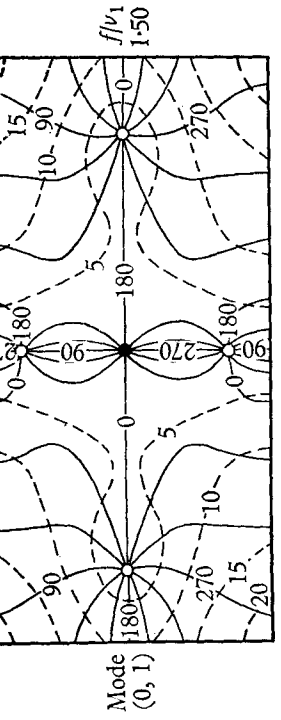

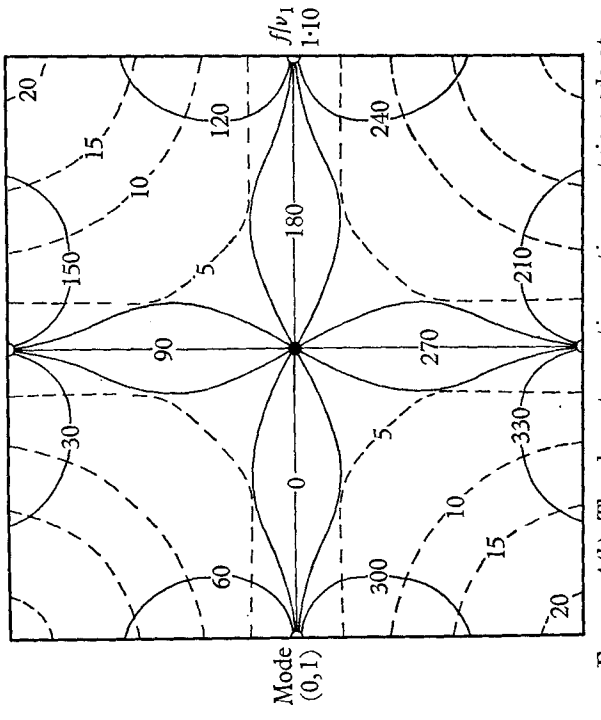

FIGURE 4 (*b*). The slowest negative antisymmetric mode at rotation higher than in figure 4 (*a*).

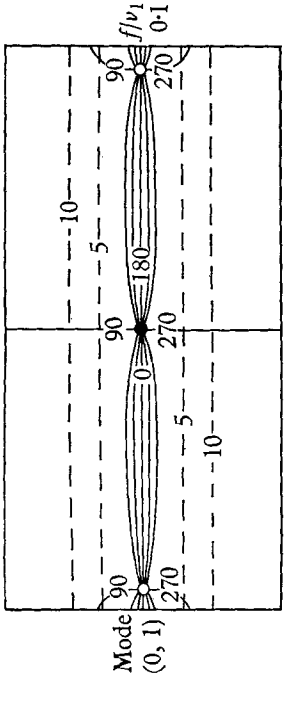

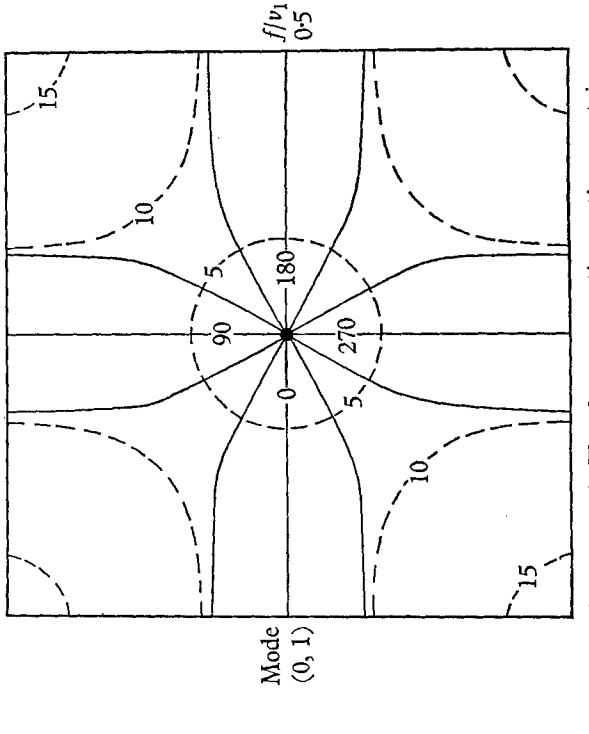

FIGURE 4 (*a*). The slowest negative antisymmetric mode at low rotation.

As the rotation increases, these points move towards the centre of the basin, and the positive wave systems associated with them eventually dominate over the central negative wave. Even though there are five amphidromic points, the arrangement is such that the central negative-wave region is surrounded by a system of three waves which travel around the boundaries in a positive direction,

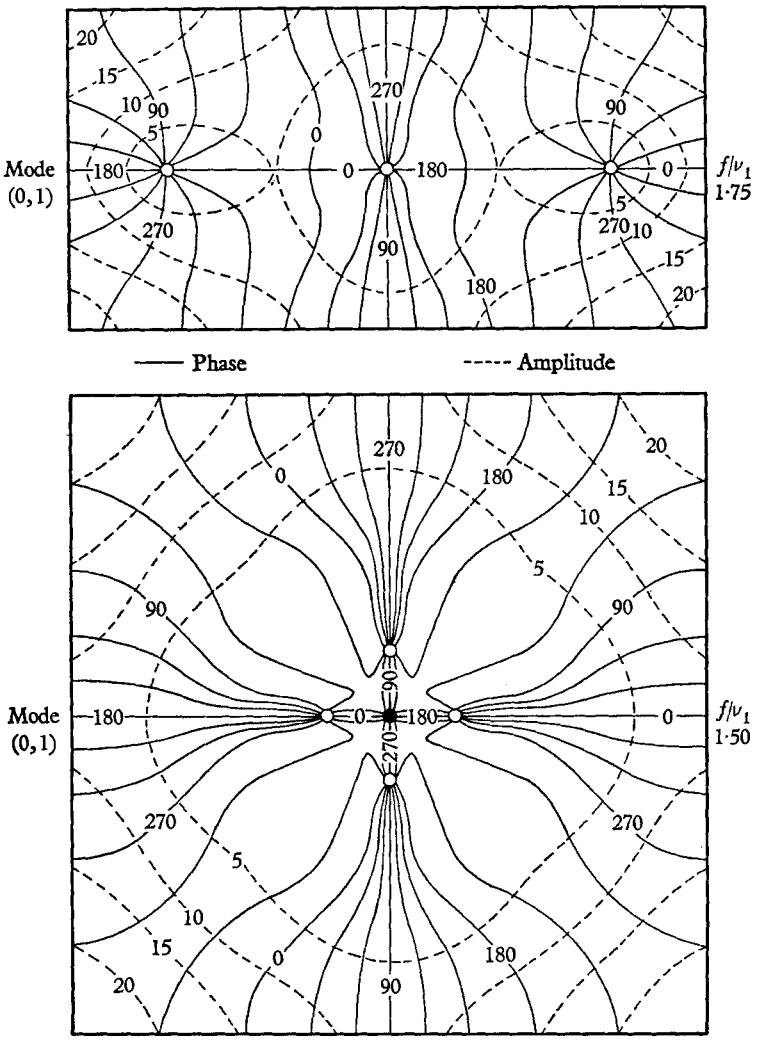

FIGURE 4(*c*). The slowest negative antisymmetric mode at rotation higher than in figure 4(*b*).

as can be seen by careful examination of the co-tidal lines of figure 4(*b*). As the rotation increases, the inner negative wave region contracts and the amplitude of this wave decreases. At $f/\nu_1 = 1{\cdot}5$ (figure 4(*c*)) the amplitude of the negative wave is practically zero. Corkan & Doodson (1952) found from their computations three positive waves and no negative wave when $\sigma/f = 1$ for this mode. However, from the present computations it does not appear that the central negative core entirely disappears in a square. Even at $f/\nu_1 = 2{\cdot}0$, for which $\sigma/f < 1$,

the negative wave is still present at the centre, but with practically negligible amplitude.

The upper parts of figures 4(*a*), (*b*) and (*c*) show the slowest negative antisymmetric mode in a 2×1 rectangle. In this case, even at the low rotation $f/\nu_1 = 0{\cdot}1$, there is one negative wave system (figure 4(*a*)) at the centre of the basin and two positive wave systems with amphidromic points located one on

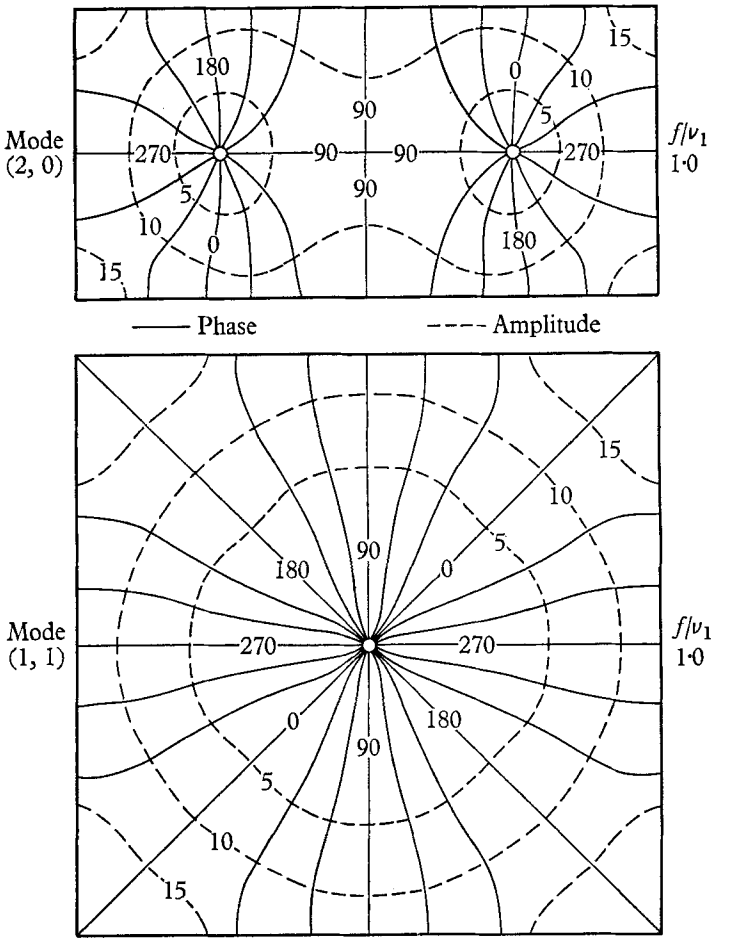

FIGURE 5. The slowest positive symmetric mode.

either side of the centre of the longitudinal axis. As the rotation is increased (figure 4(*b*)), two more positive amphidromic systems come inside the basin, one on either side of the centre on the transversal axis, for a value of f/ν_1 in the range $1{\cdot}4 < f/\nu_1 < 1{\cdot}5$. Finally by $f/\nu_1 = 1{\cdot}75$ (figure 4(*c*)) the central negative amphidromic system disappears and one has three positive waves in the basin with amphidromic points located on the longitudinal axis.

Now coming to the symmetric modes, figure 5 shows the slowest positive modes belonging to this family in a square and a rectangle. The system consists of two waves travelling in the positive direction, and the structure remains

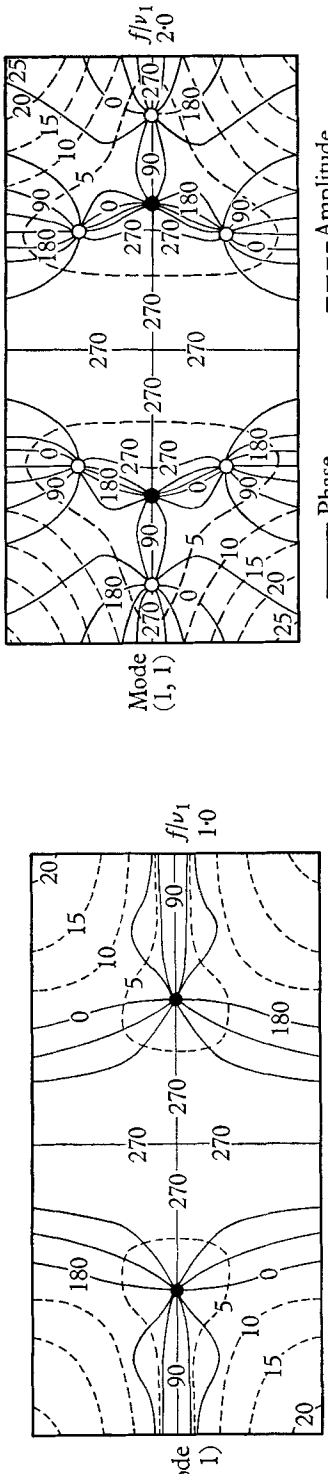

FIGURE 6 (*a*). The slowest negative symmetric mode.

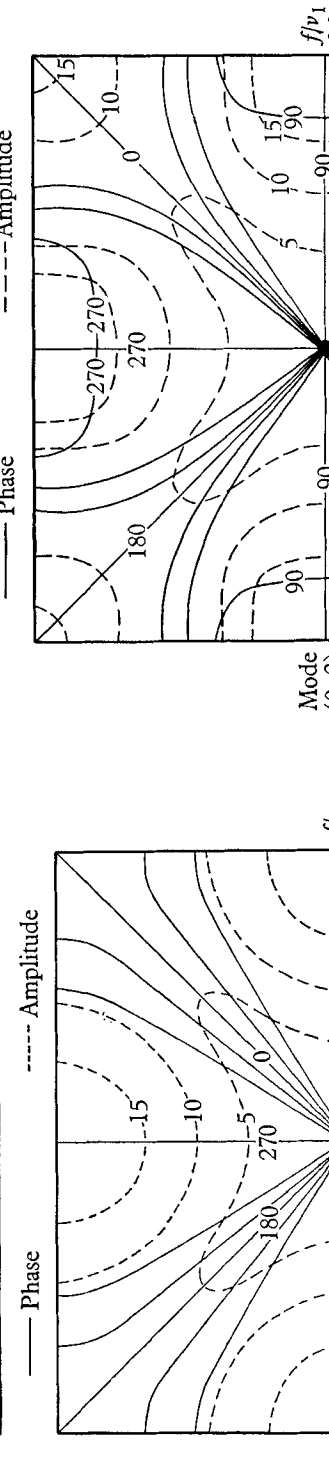

FIGURE 6 (*b*). The slowest negative symmetric mode at rotation higher than in figure 6 (*a*).

unchanged with increasing rotation. In the square both the waves travel about an amphidromic point at the centre of the basin, whereas in the rectangle each wave has a separate amphidromic point located symmetrically with respect to the centre on the longitudinal axis. At $f/\nu_1 = 1{\cdot}0$, figure 6(*a*) shows that the corresponding negatively propagating modes also consist of two waves. Just as in the case of the first negative antisymmetric mode, these modes undergo a change in structure with increase in rotation: positive amphidromic points external to the basin gradually move across the boundary into the basin. The situation when $f/\nu_1 = 2$ is shown in figure 6(*b*).

The higher modes become very complicated in their structure and hence no attempt is made to present the details here except to mention that negative amphidromic systems always appear to be 'unstable', that is, to give way to positive amphidromic systems.

In summary, it is possible to say that, for antisymmetric modes in any rectangle, the zero-rotation (1, 0) mode is transformed into the slowest positive mode and the (0, 1) mode into the slowest negative mode. For symmetric modes, the slowest zero-rotation mode of this family is transformed into a positive mode consisting of two waves. The antisymmetric modes consist of an odd number of wave systems and the symmetric modes an even number. The negative modes in all cases are 'unstable' in the sense of Corkan & Doodson. Recalling figure 2, we see that, in the case of the lowest antisymmetric and symmetric modes, the positive waves follow the low-frequency branch (along which frequency decreases with increasing rotation) and the negative waves the high-frequency branch.

In §3 we showed that the frequency of the slowest longitudinal oscillation tends to that of a Kelvin wave as the elongation of the basin increases. We now show that the structure of the oscillation also resembles that of a Kelvin wave.

Consider the zero-rotation (1, 0) mode in a rectangle and take unit amplitude for the corresponding ζ in (2.4). In the rotating case, if we assume that the transverse accelerations are small, a good approximation to the transverse slope may be obtained from the geostrophic relation as in the case of a Kelvin wave. Integration (with respect to y) of the geostrophic equation would then give the *added* surface displacement $\tilde{\zeta}$ caused by rotation. The total disturbance at any point is the sum $\zeta + \tilde{\zeta}$, which can be written

$$\zeta + \tilde{\zeta} = A(x,y)\cos[\nu t - \theta(x,y)],$$

$$A(x,y) \equiv [\cos^2 \pi a^{-1}x + c^{-2}f^2(y - \tfrac{1}{2}b)^2 \sin^2 \pi a^{-1}x]^{\frac{1}{2}},$$

$$\theta(x,y) \equiv \arctan[-c^{-1}f(y - \tfrac{1}{2}b)\tan \pi a^{-1}x],$$

where A is the amplitude and θ is the phase of high water at any point. (For details of the derivation see Defant 1961.)

The amplitudes and phases of high water along the north and south boundaries of the basin obtained from the exact analysis of the problem and from the above approximate Kelvin-wave hypothesis are shown in figure 7 for the case of $a/b = 6$ and $f/\nu_1 = 1{\cdot}0$. (The northern and southern boundaries are those parallel to the longitudinal x-axis.) Also shown for comparison is the situation in the non-rotating case. From these it is clear that there is excellent agreement

between the exact calculation of the surface profile, and the approximate Kelvin-wave calculation. The Kelvin-wave hypothesis transforms the original standing wave into an amphidromic system which rotates in a positive direction around the basin with the same period as the zero-rotation mode.

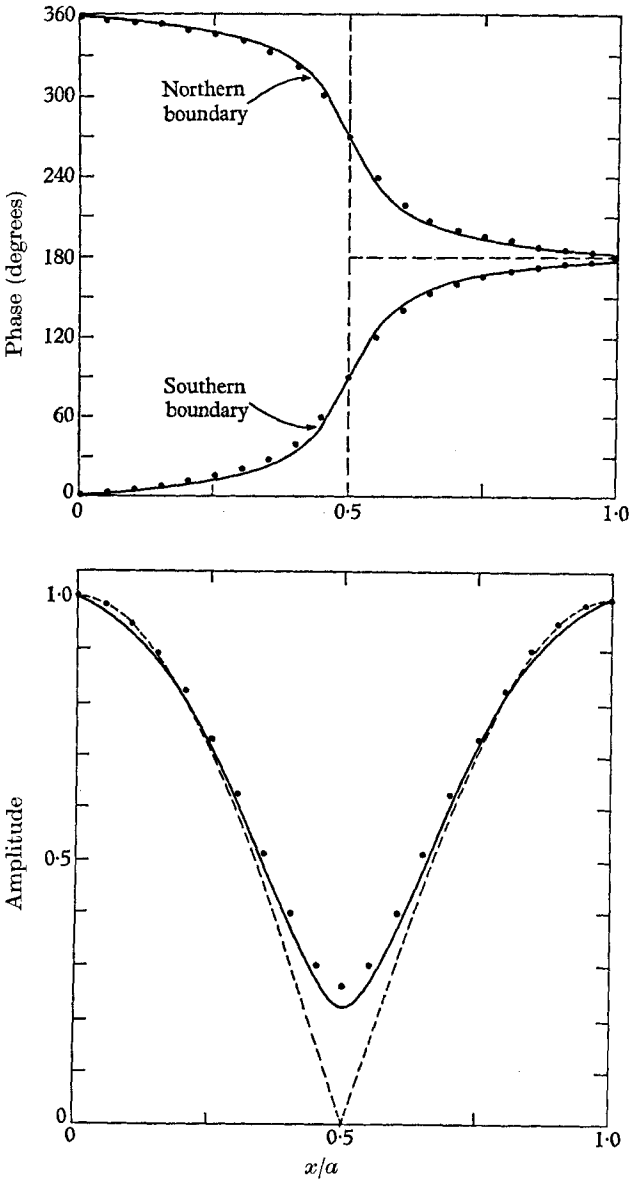

FIGURE 7. Amplitude (lower diagram) and phase of high water (upper diagram) for the slowest longitudinal oscillation on the boundaries of a 6 × 1 rectangular basin with rotation speed $f/\nu_1 = 1$. The solid line is the exact calculation, the dots are the results of applying the Kelvin-wave hypothesis and the dashed line is the situation with zero rotation.

5. Energy partition

In the zero-rotation case the total energy is partitioned equally between potential energy P and kinetic energy K of the motion (which is purely irrotational). When the potential energy is a maximum, kinetic energy is zero and vice versa. In the rotating case the kinetic energy of the motion can be resolved into two parts: $K = K^{\phi} + K^{\psi}$, where K^{ϕ} is the kinetic energy of the irrotational

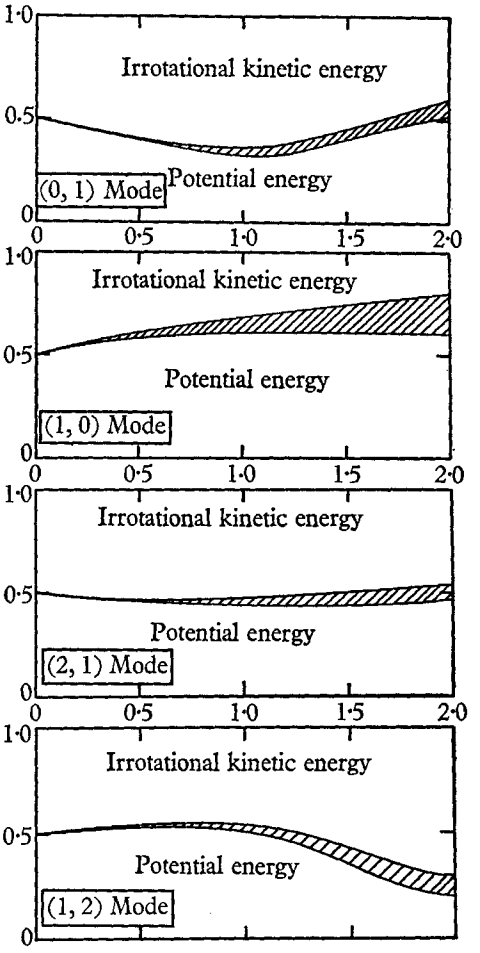

FIGURE 8. Energy partition as a function of rotation in a square basin for the modes indicated; abscissa, rotation speed f/ν_1. Shaded region represents rotational kinetic energy.

part of the motion and K^{ψ} is that of the rotational part. Moreover, at no instant can any one of P, K^{ϕ} and K^{ψ} be zero.

Figure 8 shows the partitioning of total energy between P, K^{ϕ} and K^{ψ} as a function of rotation speed f/ν_1 for some of the slowest antisymmetric modes in a square. In this figure the total energy is normalized to unity for all f/ν_1.

An inspection of figure 8 in conjunction with figure 2 shows that in modes (1, 0) (0, 1), (2, 1) (for which the computations indicate that $\sigma/f \to 0$ for large f)

the total energy primarily consists of P and K^{ψ} at large values of f. In the (2, 1) mode (which appears to belong to the case for which $\sigma/f \to 1$ for large f) the total energy seems to be partitioned primarily between K^{ψ} and K^{ϕ} for large f. Figure 8 also shows that for positive wave propagation P increases with increasing f as in the case of the (1, 0) mode as well as the (0, 1) mode for values of $f/\nu_1 > 1$.

6. Experimental results

The laboratory experiments were performed in a square tank (mean value of $a = 48{\cdot}69$ cm and $b = 48{\cdot}49$ cm). The working fluid was distilled water, to which an organic fluid 'Kodak Photoflo' was added in proportion of 10^{-3} by volume to reduce the surface tension to about 30 dynes cm^{-1}. The tank was rotated by mounting it on a turn-table and the modal generation was achieved by means of two oscillators. The amplitude response of the water-level oscillation in the tank was monitored by two wave-height probes mounted in the tank. The experimental arrangement is shown in figure 9 (plate 1). The experimental work was done for a depth given by $H/a = 0{\cdot}125$ and was limited to the slowest positive and negative antisymmetric modes and the slowest positive symmetric mode.

Table 5 gives a summary of the experimental values of σ/ν ($= T_0/T$). The values of the zero-rotation periods (T_0) are those obtained experimentally. The mean values for T_0 are

Mode	T_0 (sec)
(1, 0)	1·295
(0, 1)	1·295
(1, 1)	0·927

In table 5 the upper and lower bounds are given for the experimental estimates of T_0/T. In calculating the ratio $2\omega/\nu_1$ the value of ν_1 used is $2\pi/1{\cdot}295 = 4{\cdot}582$ rad sec^{-1}.

The arithmetic mean values of the ratio σ/ν in table 5 are plotted in figure 10, along with the corresponding theoretical curves. No corrections were applied to the theoretical periods for non-quasistatic effects, on the working assumption that these effects would be of the same order for both the rotating and non-rotating periods, and that, when the theoretical ratio σ/ν is taken, the correction factor effectively drops out. Figure 10 shows good agreement between theory and experiment. The maximum error obtained is 6 % for the (1, 0) mode at $\omega = 4$ rad sec^{-1}. However, at this speed of rotation the free surface assumes a very pronounced parabolic shape and it is not surprising that results of planar theory (which ignores the free-surface curvature) do not agree well with experimental results. The quantitative agreement between theory and experiment for the (0, 1) and (1, 1) modes is good. (The (0, 1) mode could not be generated beyond $\omega = 2$ rad sec^{-1}.)

It will be shown in part 2 that there are some modes in a rectangular basin for which $\sigma = \nu + O(\omega^2)$ in the limit of $\omega \to 0$ and some for which $\sigma = \nu + O(\omega)$. Under rotation the equilibrium configuration of the free surface is a paraboloid and the depth variation involves terms of $O(\omega^2)$. For this reason the planar

approximation, in which the free-surface curvature is ignored, is inconsistent for modes for which the frequency shift induced by rotation is also of $O(\omega^2)$. On the other hand, the planar approximation is valid, at least for small values of ω, for modes for which the frequency shift is of $O(\omega)$. A similar situation occurs

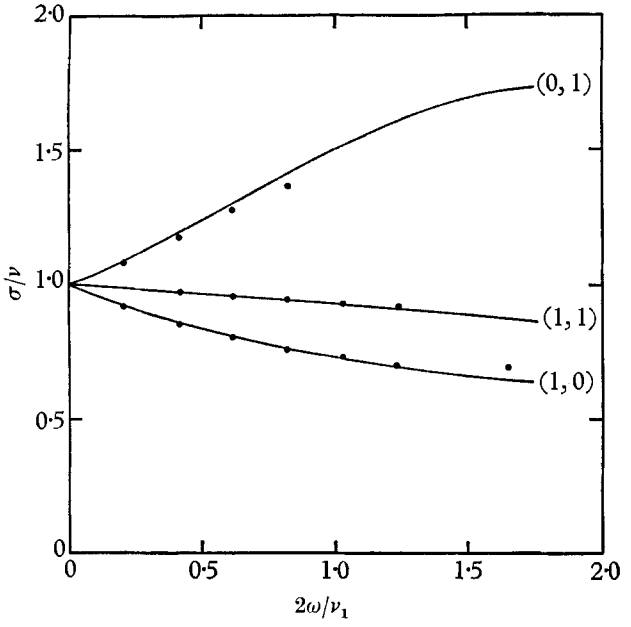

FIGURE 10. Comparison of the experimental (dots) and theoretical values of σ/ν for various speeds of rotation in a square basin.

ω (rad sec^{-1})	$2\omega/\nu_1$	Mode (1, 0)	Mode (0, 1)	Mode (1, 1)
0	0	1·0	1·0	1·0
0·5	0·206	0·920–0·917	1·084–1·082	—
1·0	0·412	0·857–0·855	1·174–1·171	0·973–0·971
1·5	0·618	0·802–0·801	1·275–1·271	0·957–0·955
2·0	0·824	0·758–0·756	1·370–1·365	0·941–0·938
2.5	1·030	0·728–0·727	—	0·925–0·921
3·0	1·237	0·703–0·701	—	0·916–0·912
4·0	1·649	0·689–0·687	—	—

TABLE 5. Experimental values of the frequency ratio σ/ν in a square tank with depth ratio $H/a = 0{\cdot}125$, as a function of rotation frequency ω, for the slowest positive antisymmetric mode (1, 0), the slowest negative antisymmetric mode (0, 1) and the slowest positive symmetric mode (1, 1)

in the case of a circular cylinder, in which the planar approximation is inconsistent for axi-symmetric modes as first pointed out by Fultz (1962), whereas it is consistent for azimuthal modes (Miles 1964).

This inconsistency in the theoretical formulation should produce a discrepancy between the theoretical and experimental results. However, a direct comparison

of the frequency values, such as that in figure 10, is not capable of bringing this fact out clearly. For this purpose, by analogy with the axi-symmetric modes in a circular cylinder (see Fultz, 1962), we define a special parameter

$$E \equiv (\sigma^2 - \nu^2)/4\omega^2. \tag{6.1}$$

In any rectangle, for those modes for which the frequency for small ω is given by $\sigma = \nu + O(\omega^2)$, we have $\sigma^2 = \nu^2 + O(\omega^2)$, and the parameter E is finite in the limit $\omega \to 0$.

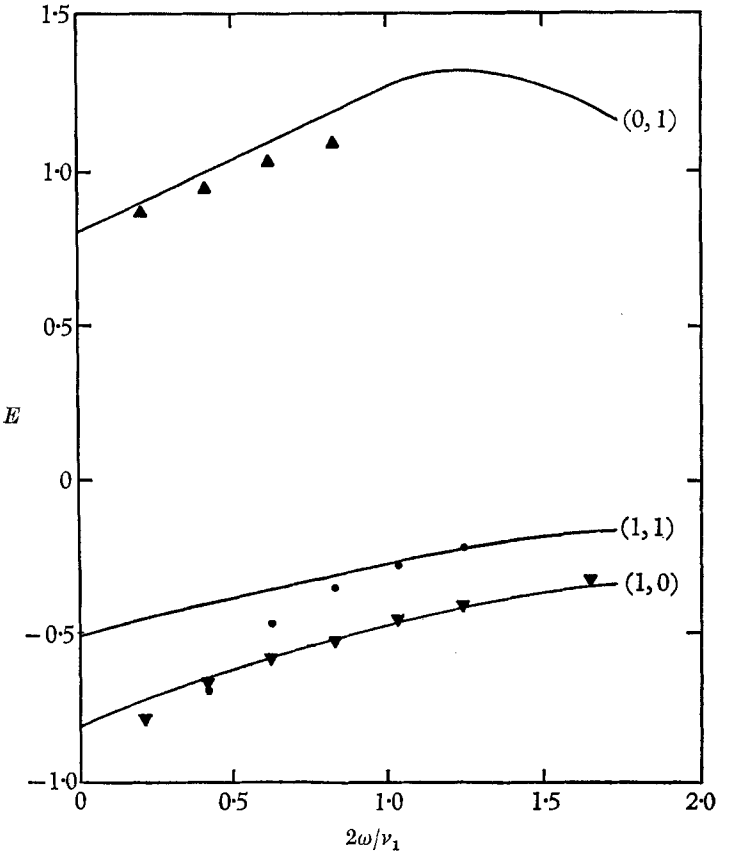

FIGURE 11. Comparison of the experimental and theoretical values of the 'ellipticity parameter' E for various speeds of rotation. The discrete points are the experimental results with ▼ for (1, 0), ▲ for (0, 1) and ● for (1, 1) modes.

On the other hand, for modes for which $\sigma = \nu + O(\omega)$, we have $\sigma^2 = \nu^2 + O(\omega)$. For this class of modes, define

$$E \equiv (\sigma^2 - \nu^2)/2\omega\nu. \tag{6.2}$$

The theoretical (planar) and experimental values of E as defined in (6.1) and (6.2) are shown in figure 11. It is seen that the agreement for the (1, 0) and (0, 1) modes (for which $\sigma = \nu + O(\omega)$) is good, but the agreement for the (1, 1) mode (for which $\sigma = \nu + O(\omega^2)$) is very poor and shows the inconsistency of the planar approximation for this class of modes.

PART 2. THEORETICAL ANALYSIS

7. The spectral-dynamic equations for a basin with arbitrary configuration

The treatment used here is based upon a method developed by Proudman (1916) whereby the equations of 'tidal' motion are transformed into a set of ordinary differential equations in an infinite sequence of purely time-dependent parameters. (Proudman's formulation shows that the parameters are analogous to the principal co-ordinates of a mechanical system having, in general, a countably infinite number of degrees of freedom.) Here we shall present only an outline of the analysis. (For details see Proudman 1916 or Rao 1965.)

The horizontal velocity $\mathbf{V}$ of a 'tidal' motion is independent of z through the complete depth H of a vertical column. If the motion takes place in a basin completely enclosed by a rigid boundary on which the normal component of $H\mathbf{V}$ is zero, then $\mathbf{V}$ can be partitioned as $\mathbf{V} = \mathbf{V}^{\phi} + \mathbf{V}^{\psi}$ in such a way that the kinetic energy is partitioned as $K = K^{\phi} + K^{\psi}$, that is,

$$\tfrac{1}{2}\rho \int \mathbf{V}^2 H\, dA = \tfrac{1}{2}\rho \int (\mathbf{V}^{\phi})^2 H\, dA + \tfrac{1}{2}\rho \int (\mathbf{V}^{\psi})^2 H\, dA,$$

where dA is an element of the basin surface area. This energy partition is essential for the subsequent analysis, and can be made if and only if $\mathbf{V}^{\phi}$ and $\mathbf{V}^{\psi}$ are expressed in terms of a velocity potential ϕ and stream function ψ, as follows:

$$\mathbf{V}^{\phi} = -\nabla\phi; \quad \mathbf{V}^{\psi} = -h^{-1}[\nabla\psi], \tag{7.1}$$

where $h \equiv H/\bar{H}$ is the non-dimensional ratio of the actual depth H to the basin mean depth $\bar{H}$, and $[\nabla\psi]$ indicates a 90-degree clockwise rotation of $\nabla\psi$ in the horizontal plane. In addition to (7.1), we also must impose boundary conditions

$$h\, \partial\phi/\partial n = 0; \quad \psi = 0. \tag{7.2}$$

It is evident from (7.1) that $\mathbf{V}^{\phi}$ is irrotational and $h\mathbf{V}^{\psi}$ is non-divergent; moreover, (7.2) requires the normal components of $h\mathbf{V}^{\phi}$ and $h\mathbf{V}^{\psi}$ to vanish *separately* on the boundary.

The determination of $\mathbf{V}^{\phi}$ and $\mathbf{V}^{\psi}$ in terms of $\mathbf{V}$ proceeds in principle by conversion of (7.1) into the inhomogeneous elliptic equations

$$\nabla . h\nabla\phi = -\nabla . h\mathbf{V}; \quad \nabla . h^{-1}\nabla\psi = \nabla . [\mathbf{V}], \tag{7.3}$$

with homogeneous boundary conditions (7.2). Since $\mathbf{V}$ is itself unknown, but must satisfy the dynamical equations (2.1) and (2.2), the actual procedure is to convert the dynamical equations into conditions upon ϕ and ψ, and, having determined ϕ and ψ in this way, to reconstruct $\mathbf{V}$ by means of (7.1). For this purpose we represent ϕ and ψ in terms of spectra of the elliptic operators which appear in (7.3). Specifically, we consider the characteristic-value problems

$$\left.\begin{aligned} -\nabla . h\nabla\phi_{\alpha} &= \lambda_{\alpha}\phi_{\alpha}, \\ h\, \partial\phi_{\alpha}/\partial n &= 0 \quad \text{on the boundary,} \end{aligned}\right\} \tag{7.4a}$$

$$\left.\begin{aligned} -\nabla . h^{-1}\nabla\psi_{\alpha} &= \mu_{\alpha}\psi_{\alpha}, \\ h^{-1}\psi_{\alpha} &= 0 \quad \text{on the boundary,} \end{aligned}\right\} \tag{7.4b}$$

where subscript α is a binary index used for spectral enumeration. The problems (7.4a) and (7.4b) are self-adjoint.† Therefore, the characteristic values λ_α and μ_α are real, and the characteristic functions ϕ_α and ψ_α are internally orthogonal sets.

Since we may choose ϕ_α and ψ_α real, the orthogonality and normalization may be stated

$$\left.\begin{aligned}\int h\mathbf{V}_\alpha^\phi.\mathbf{V}_\beta^\phi\,dA &= \lambda_\alpha\int \phi_\alpha\phi_\beta\,dA = c^2A\delta_{\alpha\beta},\\ \int h\mathbf{V}_\alpha^\psi.\mathbf{V}_\beta^\psi\,dA &= \mu_\alpha\int \psi_\alpha\psi_\beta\,dA = c^2A\delta_{\alpha\beta},\end{aligned}\right\} \tag{7.5}$$

where $c \equiv (g\bar{H})^{\frac{1}{2}}$; A is the surface area of the basin; $\delta_{\alpha\beta} = 1$ or 0 according as $\alpha-\beta = 0$ or $\neq 0$; and we define

$$\mathbf{V}_\alpha^\phi \equiv -\nabla\phi_\alpha; \quad \mathbf{V}_\alpha^\psi \equiv -h^{-1}[\nabla\psi_\alpha] \tag{7.6}$$

in harmony with (7.1). The first equality in (7.5) comes from the use of (7.4a) and (7.4b) after partial integration; the second gives the orthonormality statement.

It is appropriate now to define the (non-dimensional) expansion coefficients

$$\left.\begin{aligned}p_\alpha &\equiv \frac{1}{c^2A}\int h\mathbf{V}_\alpha^\phi.\mathbf{V}^\phi dA = \frac{1}{c^2A}\int h\mathbf{V}_\alpha^\phi.\mathbf{V}dA,\\ q_\alpha &\equiv \frac{1}{c^2A}\int h\mathbf{V}_\alpha^\psi.\mathbf{V}^\psi dA = \frac{1}{c^2A}\int h\mathbf{V}_\alpha^\psi.\mathbf{V}dA,\end{aligned}\right\} \tag{7.7}$$

for representation of $\mathbf{V}^\phi$ and $\mathbf{V}^\psi$. In view of the orthonormality (7.5), the sums on the right of

$$\left.\begin{aligned}\mathbf{V}^\phi &= \sum_\alpha p_\alpha\mathbf{V}_\alpha^\phi\\ \mathbf{V}^\psi &= \sum_\alpha q_\alpha\mathbf{V}_\alpha^\psi,\end{aligned}\right\} \tag{7.8}$$

are least-square approximations to $\mathbf{V}^\phi$ and $\mathbf{V}^\psi$. When the sums span the complete spectra of (7.4a) and (7.4b), the equality signs are valid in this sense, with the usual restrictions as to quadratic integrability and continuity of $\mathbf{V}^\phi$, $\mathbf{V}^\psi$ and their derivatives.

Having obtained orthogonal bases for $\mathbf{V}^\phi$ and $\mathbf{V}^\psi$, we must now establish a basis for the height field ζ. It can be shown by making use of the continuity equation (2.2) that the ϕ_α form a sufficient basis for the representation of ζ. For the explicit representation of ζ we choose

$$\zeta_\alpha \equiv \bar{H}c^{-1}(\lambda_\alpha)^{\frac{1}{2}}\phi_\alpha. \tag{7.9}$$

Then the orthonormality relation for the ζ_α is, by (7.5):

$$\int \zeta_\alpha\zeta_\beta\,dA = \bar{H}^2A\delta_{\alpha\beta}.$$

The corresponding expansion coefficients are non-dimensional:

$$r_\alpha \equiv \frac{1}{\bar{H}^2A}\int \zeta_\alpha\zeta\,dA, \tag{7.10}$$

† The factor h^{-1} in the boundary condition of (7.4b) imposes a more stringent condition than that in (7.2); but this is necessary to make (7.4b) self-adjoint.

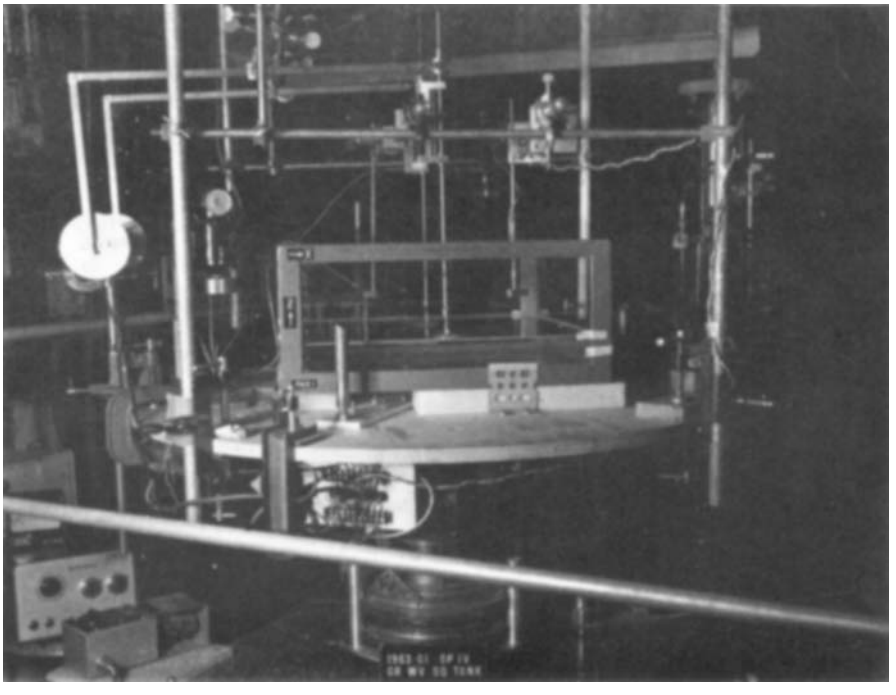

FIGURE 9. Experimental set-up showing the tank mounted on the turn-table. The oscillator arrangement and the wave-height probes also can be seen in the picture.

and give the expansion

$$\zeta = \sum_\alpha r_\alpha \zeta_\alpha. \tag{7.11}$$

It must be noted that in general the series (7.11) is not termwise differentiable at the boundaries.

Associated with the expansions (7.8) and (7.11) are the Parseval relations

$$K^\phi \equiv \tfrac{1}{2}\rho\bar{H}\int h(\mathbf{V}^\phi)^2\,dA = \tfrac{1}{2}Mc^2\sum_\alpha p_\alpha^2,$$

$$K^\psi \equiv \tfrac{1}{2}\rho\bar{H}\int h(\mathbf{V}^\psi)^2\,dA = \tfrac{1}{2}Mc^2\sum_\alpha q_\alpha^2,$$

$$P \equiv \tfrac{1}{2}\rho g\int \zeta^2\,dA = \tfrac{1}{2}Mc^2\sum_\alpha r_\alpha^2,$$

where $M \equiv \rho\bar{H}A$ is the total mass of fluid in the basin. Evidently P is the potential energy, and

$$K^\phi + K^\psi + P = \tfrac{1}{2}Mc^2\sum_\alpha (p_\alpha^2 + q_\alpha^2 + r_\alpha^2)$$

is the total energy.

Having established spectral representations of $\mathbf{V}$ and ζ in terms of p_α, q_α and r_α, we now convert the dynamical equations (2.1) and (2.2) to the spectral domain. Differentiate p_α, q_α in (7.7) and r_α in (7.10) with respect to time. Since the limits of integration (the basin boundaries) are assumed to be independent of t, and since the characteristic functions $\mathbf{V}_\alpha^\phi$, $\mathbf{V}_\alpha^\psi$, ζ_α also are independent of t, the result of this differentiation is merely to introduce $\partial\mathbf{V}/\partial t$ in place of $\mathbf{V}$ in (7.7), and $\partial\zeta/\partial t$ in place of ζ in (7.10). The governing equations (2.1), (2.2) may then be used to eliminate $\partial\mathbf{V}/\partial t$ and $\partial\zeta/\partial t$. On doing this and making use of (7.4) and (7.6)–(7.9), the result after some partial integrations may be written:

$$\left.\begin{aligned} dp_\alpha/dt &= \nu_\alpha r_\alpha + f\sum_\beta (a_{\alpha\beta}p_\beta + b_{\alpha\beta}q_\beta),\\ dq_\alpha/dt &= \quad\; f\sum_\beta (c_{\alpha\beta}p_\beta + d_{\alpha\beta}q_\beta),\\ \text{and}\qquad dr_\alpha/dt &= -\nu_\alpha p_\alpha. \end{aligned}\right\} \tag{7.12}$$

Here the following symbols are defined:

$$\left.\begin{aligned} \nu_\alpha &\equiv (c^2\lambda_\alpha)^{\frac{1}{2}},\\ a_{\alpha\beta} \equiv \{\mathbf{V}_\alpha^\phi, [\mathbf{V}_\beta^\phi]\}, &\quad c_{\alpha\beta} \equiv \{\mathbf{V}_\alpha^\psi, [\mathbf{V}_\beta^\phi]\},\\ b_{\alpha\beta} \equiv \{\mathbf{V}_\alpha^\phi, [\mathbf{V}_\beta^\psi]\}, &\quad d_{\alpha\beta} = \{\mathbf{V}_\alpha^\psi, [\mathbf{V}_\beta^\psi]\}, \end{aligned}\right\} \tag{7.13}$$

where we use the notation

$$\{\mathbf{U}, \mathbf{V}\} \equiv c^{-2}A^{-1}\int h\mathbf{U}.\mathbf{V}\,dA$$

to represent the inner product of any two vectors $\mathbf{U}$, $\mathbf{V}$. The coupling coefficients defined in (7.13) are numerical constants which depend only upon the geometry of the basin and are completely determined by the solutions ϕ_α, ψ_α of the characteristic-value problems (7.4). Moreover,

$$a_{\alpha\beta} = -a_{\beta\alpha} \quad \text{and} \quad b_{\alpha\beta} = -c_{\beta\alpha}, \tag{7.14}$$

as is evident from the definitions.

It is apparent from (7.12) that ν_α is the frequency of the normal modes in the zero-rotation case ($f = 0$). Rotation introduces a coupling between the set of p_α and the set of q_α, so that, when $f \neq 0$, the normal modes can be built up only through linear combinations of the sets $p_\alpha, q_\alpha, r_\alpha$. Equations (7.12) correspond to those derived by Proudman (1916).

8. The spectral-dynamic equations for a rectangular basin of uniform depth

The treatment thus far has been applicable to a basin of arbitrary shape and depth. We now specialize the problem for the case of a rectangular basin of uniform depth ($h = 1$). Consider a rectangle $0 \leqslant x \leqslant a$ and $0 \leqslant y \leqslant b$, where a and b are the lengths of the long and short sides ($a \geqslant b$). Then with $h = 1$ the normalized solution of the Neumann problem (7.4a) is

$$\left.\begin{aligned} \phi_\alpha &= \epsilon_\alpha c \lambda_\alpha^{-\frac{1}{2}} \cos(k\pi x/a) \cos(l\pi y/b), \\ \lambda_\alpha &= \pi^2(k^2/a^2 + l^2/b^2), \end{aligned}\right\} \tag{8.1}$$

where ϵ_α determined in accordance with (7.5) is equal to $\sqrt{2}$ or 2 according as $kl = 0$ or $\neq 0$. Here $\alpha \equiv (k, l)$ and k, l are any two integers, positive or zero (negative values being redundant). (The trivial case $k = 0 = l$ is excluded.) The wave-number vector is, strictly, $\pi(k/a, l/b)$; however, since in a given problem a and b are fixed, it is more convenient to focus attention upon the integer pair k, l which specifies the variable part of the wave-number.

For the Dirichlet problem (7.4b), the normalized solution is

$$\left.\begin{aligned} \psi_\alpha &= 2c\mu_\alpha^{-\frac{1}{2}} \sin(k\pi x/a) \sin(l\pi y/b), \\ \mu_\alpha &= \pi^2(k^2/a^2 + l^2/b^2), \end{aligned}\right\} \tag{8.2}$$

where $\alpha \equiv (k, l)$ as in (8.1).

The characteristic functions ϕ_α, ψ_α in (8.1), (8.2) have certain symmetry properties which it is important to elucidate. If $F(x, y)$ is any position function defined over the rectangle, we say that it is

$$\left.\begin{aligned} &\text{antisymmetric if } F(a-x, b-y) = -F(x, y), \\ &\text{symmetric if } F(a-x, b-y) = +F(x, y), \end{aligned}\right\} \tag{8.3}$$

for all x, y. Then from (8.1) and (8.2) it can be seen that ϕ_α, ψ_α are

$$\left.\begin{aligned} &\text{antisymmetric if } k+l \text{ is odd}, \\ &\text{symmetric if } k+l \text{ is even}. \end{aligned}\right\} \tag{8.4}$$

It is important to note that alternatives (8.4) apply to all ϕ_α, ψ_α.

If F in (8.3) is symmetric, ∇F is antisymmetric and vice versa. Moreover, the product of any two functions is symmetric if the functions have the same symmetry, and is antisymmetric if they have opposite symmetry. Consequently, from the definitions of the coupling coefficients given in (7.13), it follows that (with $h = 1$) $a_{\alpha\beta}$ vanishes if α and β have opposite symmetry, since then $\nabla\phi_\alpha \cdot [\nabla\phi_\beta]$ is antisymmetric and the integral of an antisymmetric function over the rectangle is clearly zero. Similar considerations apply to the other

coupling coefficients. We come therefore to the important conclusion that *in the spectral-dynamic equations* (7.12), p_α *cannot be coupled to either* p_β *or* q_β *and* q_α *cannot be coupled to* p_β *or* q_β *unless* α *and* β *belong to elements having the same symmetry*. This means that the functions ϕ_α and ψ_α are either all symmetric or all antisymmetric. Another way to state this conclusion is : *the normal modes of free oscillation in a rectangular basin are either symmetric or antisymmetric* (Taylor 1922).

The foregoing discussion shows that the complete set of spectral elements (8.1) or (8.2) can be divided into two mutually exclusive, 'uncoupled' subsets on the basis of the type of symmetry defined in (8.3). Within each of these subsets a further subdivision can be made, which also has an important bearing on the coupling between spectral elements as will now be explained.

We have seen that $k+l$ must be odd for all spectral elements of an antisymmetric mode. This parity can occur in one of two ways: k odd and l even, or k even and l odd. It will be convenient to use a prime to identify elements of the latter group, so that henceforth

$$\left.\begin{array}{c} \textit{for antisymmetric elements} \\ \alpha \equiv (k,l) \text{ means } k \text{ odd, } l \text{ even;} \\ \alpha' \equiv (k',l') \text{ means } k' \text{ even, } l' \text{ odd.} \end{array}\right\} \tag{8.5}$$

The importance of this grouping of antisymmetric elements comes from the fact that there can be no coupling between two elements if both are in the α-group or if both are in the α'-group.

To prove the latter statement, it is necessary to examine additional symmetry properties of the characteristic functions. In particular, a function $F(x,y)$ can have x-symmetry $(+)$ or x-antisymmetry $(-)$ according as

$$F(a-x,y) = \pm F(x,y).$$

Similarly, it has y-symmetry or -antisymmetry according as

$$F(x,b-y) = \pm F(x,y).$$

It is easy to see from (8.1) and (8.2) that, with α and α' as in (8.5), ϕ_α and $\psi_{\alpha'}$ have x-antisymmetry and y-symmetry, whereas $\phi_{\alpha'}$ and ψ_α have x-symmetry and y-antisymmetry. (Evidently all of these functions have joint (x,y) antisymmetry in the sense of (8.3).) On this basis, it can be shown directly from (7.13) that all coupling coefficients vanish if the coupling is of the type α, β or α', β'.

Similar considerations apply to the symmetric modes. By (8.4), symmetric modes are built up from spectral elements for which $k+l$ is even, so by analogy with (8.5) we adopt the convention that

$$\left.\begin{array}{c} \textit{for symmetric elements} \\ \alpha \equiv (k,l) \text{ means } k \text{ odd, } l \text{ odd;} \\ \alpha' \equiv (k',l') \text{ means } k' \text{ even, } l' \text{ even.} \end{array}\right\} \tag{8.6}$$

From considerations of x-symmetry and y-symmetry, exactly as in the case of antisymmetric modes, we find that all coupling coefficients between symmetric elements vanish if the coupling is of the type α, β or α', β'.

We have now divided the complete set of spectral elements (8.1) and (8.2) into four subsets, two of which are antisymmetric (α and α' as in (8.5)) and two symmetric (α and α' as in (8.6)). There is no coupling between antisymmetric and symmetric elements, and there is no coupling of type α, β or α', β'. It follows that for either antisymmetric or symmetric modes the spectral-dynamic equations (7.12) can be written separately for α-elements and α'-elements as follows

$$\left.\begin{aligned} dp_\alpha/dt &= \nu_\alpha r_\alpha + f\sum_{\alpha'}(a_{\alpha\alpha'}p_{\alpha'} + b_{\alpha\alpha'}q_{\alpha'}),\\ dq_\alpha/dt &= f\sum_{\alpha'} c_{\alpha\alpha'}p_{\alpha'},\\ dr_\alpha/dt &= -\nu_\alpha p_\alpha, \end{aligned}\right\} \tag{8.7a}$$

$$\left.\begin{aligned} dp_{\alpha'}/dt &= \nu_{\alpha'}r_{\alpha'} + f\sum_{\alpha'}(a_{\alpha'\alpha}p_\alpha + b_{\alpha'\alpha}q_\alpha),\\ dq_{\alpha'}/dt &= f\sum_{\alpha} c_{\alpha'\alpha}p_\alpha \end{aligned}\right\} \tag{8.7b}$$

and

$$dr_{\alpha'}/dt = -\nu_{\alpha'}p_{\alpha'}.$$

The middle equation in each of these sets has been simplified by introducing the fact that for a basin of uniform depth all coupling coefficients of the d-type in (7.13) are zero.

In (8.7) there are, formally, six types of coupling coefficients. However, according to (7.14) we have

$$a_{\alpha'\alpha} = -a_{\alpha\alpha'}; \quad b_{\alpha'\alpha} = -c_{\alpha\alpha'}; \quad c_{\alpha'\alpha} = -b_{\alpha\alpha'}, \tag{8.8}$$

so the three types required in (8.7b) are in fact expressible in terms of the three required in (8.7a). By direct substitution of (8.1) and (8.2) into the definitions (7.13), the following explicit formulae are found for coupling coefficients applicable to a rectangular basin of uniform depth:

$$a_{\alpha\alpha'} = \frac{4\epsilon_\alpha\epsilon_{\alpha'}(k'^2l^2 - k^2l'^2)}{ab\lambda_\alpha^{\frac{1}{2}}\lambda_{\alpha'}^{\frac{1}{2}}(k^2-k'^2)(l^2-l'^2)},$$

$$b_{\alpha\alpha'} = -\frac{8\epsilon_\alpha\lambda_\alpha^{\frac{1}{2}}k'l'}{\pi^2\mu_{\alpha'}^{\frac{1}{2}}(k^2-k'^2)(l^2-l'^2)},$$

$$c_{\alpha\alpha'} = \frac{8\epsilon_{\alpha'}\mu_{\alpha'}^{\frac{1}{2}}kl}{\pi^2\lambda_\alpha^{\frac{1}{2}}(k^2-k'^2)(l^2-l'^2)}.$$

In deriving these results, use is made of the fact that $k+k'$ and $l+l'$ are of odd parity, according to (8.5) and (8.6). It should be noted that the rectangle dimensions a, b enter the preceding formulae only through the ratio a/b. This can be seen by examining the expressions for λ_α and μ_α in (8.1) and (8.2). From these expressions it is also evident that $\lambda_\alpha = \mu_\alpha$.

In working toward a solution of the spectral-dynamic equations (8.7), it is necessary to order each of the sets α and α' as a one-dimensional array. The specific order in which the elements of these sets are arranged is somewhat arbitrary, and will be considered later. At present it suffices to assume that an ordering has been assigned to the elements of each set. We shall signify this ordering by

means of scalar indices $i = 1, 2, 3, \ldots$ or $j = 1, 2, 3, \ldots$. However, to avoid cumbersome double subscripts an abbreviated notation will be used henceforth, exemplified by the following:

$$p_i \equiv p_{\alpha_i}, \quad p'_i \equiv p_{\alpha'_i}, \quad a_{ij} \equiv a_{\alpha_i \alpha_j}.$$

On this understanding it is evident that the spectral equations (8.7) can be written (making use of (8.8)) in the following matrix form:

$$\left.\begin{aligned} d\mathbf{p}/dt &= \langle \nu \rangle \mathbf{r} + f(\mathbf{A}\mathbf{p}' + \mathbf{B}\mathbf{q}') \\ d\mathbf{q}/dt &= f\mathbf{C}\mathbf{p}', \\ d\mathbf{r}/dt &= -\langle \nu \rangle \mathbf{p}; \end{aligned}\right\} \tag{8.9a}$$

$$\left.\begin{aligned} d\mathbf{p}'/dt &= \langle \nu' \rangle \mathbf{r}' - f(\mathbf{A}^T\mathbf{p} + \mathbf{C}^T\mathbf{q}), \\ d\mathbf{q}'/dt &= -f\mathbf{B}^T\mathbf{p}, \\ d\mathbf{r}'/dt &= -\langle \nu' \rangle \mathbf{p}'. \end{aligned}\right\} \tag{8.9b}$$

Here we have introduced vector and matrix notation, exemplified by

$$\begin{aligned} \mathbf{p} &\equiv \operatorname{col} p_i \\ \langle\,\rangle &\equiv \text{diagonal matrix} \\ \mathbf{A} &\equiv \|a_{ij}\|. \end{aligned}$$

In (8.9*b*), the superscipt T means a matrix transpose.

Since we seek the normal modes, we assume that the time-dependent vectors of (8.9) have the form

$$\left.\begin{aligned} (\mathbf{p}, \mathbf{q}, \mathbf{r}') &= (\mathbf{P}, \mathbf{Q}, \mathbf{R}') \sin \sigma t, \\ (\mathbf{p}', \mathbf{q}', \mathbf{r}) &= (\mathbf{P}', \mathbf{Q}', \mathbf{R}) \cos \sigma t, \end{aligned}\right\} \tag{8.10}$$

where σ is the normal-mode frequency, and the vectors denoted by capital letters on the right are constants to be determined. Substitute this in (8.9) and eliminate $\mathbf{Q}$, $\mathbf{Q}'$, $\mathbf{R}$, $\mathbf{R}'$. The result is:

$$\left.\begin{aligned} (\sigma^2\mathbf{I} - \langle \nu^2 \rangle - f^2\mathbf{B}\mathbf{B}^T)\,\mathbf{P} - \sigma f \mathbf{A}\mathbf{P}' &= 0, \\ -\sigma f \mathbf{A}^T\mathbf{P} + (\sigma^2\mathbf{I} - \langle \nu'^2 \rangle - f^2\mathbf{C}^T\mathbf{C})\mathbf{P}' &= 0. \end{aligned}\right\} \tag{8.11}$$

Here $\mathbf{I}$ is the identity matrix. If a solution of (8.11) is found, the corresponding normal-mode configuration can be obtained from insertion of (8.10) into (7.8) and (7.11).

If we take $\cos \sigma t$ in place of $\sin \sigma t$ in (8.10) and $\sin \sigma t$ in place of $\cos \sigma t$, then the result is (8.11) with σ replaced by $-\sigma$. The equations thus modified evidently have the solution

$$-\sigma, -\mathbf{P}, -\mathbf{Q}, \mathbf{R}; \quad \mathbf{P}', \mathbf{Q}', -\mathbf{R}',$$

and it can be verified that the corresponding normal-mode configuration would be identical with the one obtained from (8.10) except for a quarter-period phase shift of t. A linear combination of the two configurations would again give the configuration corresponding to (8.10) but with an arbitrary phase angle for t. There is no loss of generality in taking this phase angle to be zero: that is, in restricting attention to the phase imposed by (8.10). In other words, although the admissible values of σ occur in pairs $\pm|\sigma|$, there is no loss of generality in restricting attention to $+|\sigma|$ because $-|\sigma|$ corresponds to a normal mode with the same configuration as $+|\sigma|$ but with a phase shift of a quarter period.

In (8.11) one more elimination (of $\mathbf{P}$ or $\mathbf{P}'$) is possible, but it has been found more convenient to solve (8.11) jointly for $\mathbf{P}$ and $\mathbf{P}'$, so the admissible values of σ evidently are the roots of

$$\det \mathbf{L}(\sigma) = 0, \tag{8.12}$$

$$\mathbf{L}(\sigma) \equiv \left(\begin{array}{c|c} \sigma^2\mathbf{I} - \langle\nu^2\rangle - f^2\mathbf{B}\mathbf{B}^T & -\sigma f\mathbf{A} \\ \hline -\sigma f\mathbf{A}^T & \sigma^2\mathbf{I} - \langle\nu'^2\rangle - f^2\mathbf{C}^T\mathbf{C} \end{array}\right).$$

It is evident that the coefficient matrix $\mathbf{L}$ is symmetric.

9. Numerical computation of frequencies and modal configurations

In order to proceed with the determination of the admissible values of σ according to (8.12), it is necessary at this stage to decide upon a specific ordering of the wave-number pairs (k, l) and (k', l'). This we have done in such a manner that the zero-rotation frequencies ν_i and ν_i' form a sequence of ascending values; that is, $\nu_1 < \nu_2 < \nu_3 \ldots$ and $\nu_1' < \nu_2' < \nu_3' \ldots$. Even though this ordering is arbitrary to some extent, it is plausible because we are mainly interested in determining the effect of rotation on the first few slowest modes. Since $\mathbf{L}(\sigma)$ must be truncated at some point for computational purposes, this particular ordering takes into account the slowest modes contained in the zero-rotation spectrum.

The truncation of $\mathbf{L}(\sigma)$ means a truncation of the vectors $\mathbf{P}$, $\mathbf{P}'$ and hence of $\mathbf{Q}$, $\mathbf{Q}'$, $\mathbf{R}$, $\mathbf{R}'$ also. Although the truncated $\mathbf{P}$, $\mathbf{P}'$, $\mathbf{Q}$, $\mathbf{Q}'$ need not have the same number of elements, we have in fact given $\mathbf{P}$ and $\mathbf{P}'$ the same number of elements in all numerical computations. (If $\mathbf{P}$ and $\mathbf{P}'$ are truncated at the first element, (8.12) gives the result (1.1) of Lamb.) The roots σ of (8.12) were calculated by an application of the rule of false position. Once a root σ is found, the associated vector $(\mathbf{P}, \mathbf{P}')$ is obtained, and then the vectors $\mathbf{Q}$, $\mathbf{Q}'$, $\mathbf{R}$, $\mathbf{R}'$ by means of (8.9).

The modal configuration is represented in terms of the phase and amplitude of the height field. The solution for ζ obtained from (7.11) and (8.10) may be written

$$\zeta(x, y, t) = A(x, y) \cos[\sigma t - \theta(x, y)],$$

$$A(x, y) \equiv \{[\sum_i R_i \zeta_i(x, y)]^2 + [\sum_i R_i' \zeta_i'(x, y)]^2\}^{\frac{1}{2}},$$

$$\theta(x, y) \equiv \arctan[\sum_i R_i' \zeta_i'(x, y) / \sum_i R_i \zeta_i(x, y)].$$

A is the amplitude and θ is the phase of high water at any point in the rectangle. These quantities are calculated at intervals of $\Delta x = 0{\cdot}025a = \Delta y$.

The frequencies were computed by truncating $\mathbf{L}(\sigma)$ at 20×20 size for

$$f/\nu_1 = 0{\cdot}25\,(0{\cdot}25)\,1{\cdot}00,$$

at 24×24 for $f/\nu_1 = 1{\cdot}25\,(0{\cdot}25)\,1{\cdot}50$, at 28×28 for $f/\nu_1 = 1{\cdot}75\,(0{\cdot}25)\,2{\cdot}25$. Table 6 shows the convergence of σ/ν_1 for the slowest positive and negative antisymmetric modes (which, in general, are the most affected by rotation) as a function of the size of $\mathbf{L}(\sigma)$. From this table it is clear that the maximum change in σ is about $0{\cdot}1\,\%$ for $f/\nu_1 = 1$ and $0{\cdot}3\,\%$ for $f/\nu_1 = 2$. Moreover, from an examination of the components of $\mathbf{P}$ and $\mathbf{P}'$ it can be inferred that inclusion of more terms in $\mathbf{L}(\sigma)$ is not likely to produce any significant change in σ. Similar results for the higher modes are not presented here but a test of the convergence property at $f/\nu_1 = 1$

showed even better convergence for these modes. In the case of a 2×1 rectangle with $f/\nu_1 = 2$, it was found that $\sigma/\nu_1 = 0{\cdot}8567$ from a 24×24 determinant and $0{\cdot}8572$ from a 28×28. Taylor's (1922) result for this case is $0{\cdot}859$.

It is clear from this brief summary that the frequency results obtained by truncating $\mathbf{L}(\sigma)$ at the sizes indicated in the earlier part of the preceding paragraph represent values that have converged well, at least up to three significant digits.

		Determinant size		
Mode	f_1/ν_1	16×16	20×20	24×24
(1, 0)	1	0·7225	0·7234	0·7231
(0, 1)	1	1·5089	1·5088	1·5088
		Determinant size		
Mode	f/ν_1	24×24	28×28	30×30
(1, 0)	2	0·6163	0·6166	0·6181
(0, 1)	2	1·7337	1·7386	1·7368

TABLE 6. Values of σ/ν_1 from convergence test for a square basin

10. The zero-rotation limit of the normal-mode solutions

By means of the numerical procedure described in the preceding section, it is possible to obtain the frequencies for any rotation speed f. However, in the limit $f \to 0$ it is possible to obtain analytic results. We shall briefly state the results for

$$\left(\frac{\partial\sigma}{\partial f}\right)_{f=0} \quad \text{and} \quad \left(\frac{\partial^2\sigma}{\partial f^2}\right)_{f=0}.$$

Such results are useful and, moreover, have played an important role in the historical development of the subject.

Starting from the infinite set of homogeneous equations (8.11) for P_i and P'_j we can obtain three set of equations—namely (8.11) evaluated at $f = 0$, and the equations once and twice differentiated with respect to f and evaluated at $f = 0$.

The inferences from these derived sets of equations depend upon whether the zero-rotation limit of σ coincides with a singlet (non-repeated) zero-rotation frequency and, if not, upon the nature of the multiplicity. In the case of a mode whose zero-rotation frequency is a singlet ν_r, equations (8.11) evaluated at $f = 0$ show that except for the element P_r all the elements of $\mathbf{P}$ are zero and all the elements of $\mathbf{P}'$ are zero. Since we consider only free modes, we can assign $P_r = 1$ for all f, arbitrarily. The once-differentiated equations of (8.11) (again evaluated at $f = 0$) then show that $\partial\sigma/\partial f = 0$ at $f = 0$. Proceeding to the twice-differentiated equations of (8.11), one can obtain $\partial^2\sigma/\partial f^2$ at $f = 0$. The results obtained thus are

$$\sigma = \nu_r; \quad \partial\sigma/\partial f = 0, \tag{10.1}$$

$$\frac{\partial^2\sigma}{\partial f^2} = \sum_j \left(\frac{\sigma a_{rj}^2}{\sigma^2 - \nu_j'^2} + \sigma^{-1} b_{rj}^2\right); P_r = 1 \quad \text{for all} \quad f$$

at $f = 0$. (It is also possible to obtain results for $\partial\mathbf{P}/\partial f$, $\partial^2\mathbf{P}/\partial f^2$, $\partial\mathbf{P}'/\partial f$, $\partial^2\mathbf{P}'/\partial f^2$ from the equations derived from (8.11); see Rao 1965.)

Thus, in the case of a singlet the effect of rotation is $O(f^2)$ on the frequency σ, since in the limit $f = 0$ we find $\partial\sigma/\partial f = 0$ and $\partial^2\sigma/\partial f^2 \neq 0$. In figure 2, this is exemplified by modes (1, 1), (2, 2) in a square and all the modes with the exception of (0, 2) and (4, 0) in a 2×1 rectangle, all of which have zero slope at $f = 0$.

The result (10.1) corresponds to the corrected form of the classical result of Rayleigh (1909) (this correction was made by Proudman (1933); see also Veltkamp (1960)). The result (10.1) specialized to the (1, 0) mode in a 2×1 rectangle also corresponds to the explicit result given by Van Dantzig & Lauwerier (1960); their formula is given by equation (1.4) in this paper.

Now consider a mode whose zero-rotation frequency coincides with a multiplet of the non-rotating spectrum. In this case the inferences from the derived equations from (8.11) depend upon whether the elements of the multiplet belong to the same modal species; that is, upon whether or not all elements have the same symmetry in x. If they do, we shall refer to the multiplet as 'homogeneous'; if not, 'heterogeneous'. Suppose first that we have a homogeneous multiplet of arbitrary order, and let subscripts $r, s, t, \ldots$ identify the elements in question, so that $\sigma = \nu_r = \nu_s = \nu_t = \ldots$. Then a straightforward analysis of the derived equations yields:

$$\left.\begin{aligned} \sigma = \nu_r = \nu_s = \nu_t = \ldots;\ \partial\sigma/\partial f = 0, \\ \partial^2\sigma/\partial f^2 = \text{eigenvalues of } \|g_{mn}\|, \\ (P_r, P_s, P_t, \ldots) = \text{eigenvectors of } \|g_{mn}\|, \end{aligned}\right\} \tag{10.2}$$

where g_{mn} are the symmetric matrix elements

$$g_{mn} \equiv \frac{1}{\sigma}\sum_j \left(\frac{\sigma^2 a_{mj}a_{nj}}{\sigma^2 - \nu_j'^2} + b_{mj}b_{nj}\right).$$

The indices m, n range over all elements $r, s, t, \ldots$ of the multiplet. Hence in the zero-rotation limit $\mathbf{P}$ has a finite number of non-zero components, one for each element of the multiplet. A comparison of (10.1) with (10.2) shows that in both cases σ is $O(f^2)$. In figure 2, the case of a homogeneous doublet is exemplified by modes (2, 0), (0, 2); (1, 3), (3, 1) in a square and (0, 2), (4, 0) in a 2×1 rectangle.

Consider the case of heterogeneous multiplicities. In the simple case of a doublet ($\sigma = \nu_r = \nu_s'$) we obtain at $f = 0$:

$$\left.\begin{aligned} \sigma = \nu_r = \nu_s', \\ \partial\sigma/\partial f = \pm\tfrac{1}{2}a_{rs}, \end{aligned}\right\} \tag{10.3a}$$

$$\left.\begin{aligned} \frac{\partial^2\sigma}{\partial f^2} = \sum_{i\neq r}\left(\frac{\sigma a_{is}^2}{\sigma^2 - \nu_i^2} + \sigma^{-1}c_{is}^2\right) + \sum_{j\neq r}\left(\frac{\sigma a_{rj}^2}{\sigma^2 - \nu_j'^2} + \sigma^{-1}b_{rj}^2\right) \\ + \sigma^{-1}(\tfrac{1}{2}a_{rs}^2 + b_{rs}^2 + c_{rs}^2), \\ (P_r, P_s') = (1, 1) \quad \text{for} \quad \partial\sigma/\partial f = +\tfrac{1}{2}a_{rs}, \\ (P_r, P_s') = (-1, 1) \quad \text{for} \quad \partial\sigma/\partial f = -\tfrac{1}{2}a_{rs}. \end{aligned}\right\} \tag{10.3b}$$

Hence when $f = 0$, $\mathbf{P}$ and $\mathbf{P}'$ have one non-zero component. A comparison of (10.3) for the heterogeneous doublet with (10.1) for a singlet (or (10.2) for homogeneous multiplet) shows an important difference between the two cases. For the

case of heterogeneous multiplicities in the zero-rotation frequency spectrum, the effect of rotation on the frequency σ is of $O(f)$ since $\partial\sigma/\partial f \neq 0$ at $f = 0$, whereas for the homogeneous case, the effect is of $O(f^2)$. The case of a heterogeneous doublet is exemplified by modes (1, 0), (0, 1); (1, 2), (2,1); (3, 0), (0, 3) in a square basin in figure 2.

The result (10.3*a*) corresponds to the corrected result of Rayleigh (1903). The results (10.3*a*, *b*) were given by Van Dantzig & Lauwerier (1960) in the special case of the (1, 0) and (0, 1) modes in a square; their formula is given by equation (1.3) in this paper.

The case of a heterogeneous multiplet of aribtrary order $N+N'$ can be worked out with little difficulty. In particular, let

$$\sigma\begin{cases} = \nu_r = \nu_s = \nu_t = \ldots & (N \text{ values}), \\ = \nu'_{r'} = \nu'_{s'} = \nu'_{t'} = \ldots & (N' \text{ values}), \end{cases}$$

at the zero-rotation limit. Then it can be shown that the $N+N'$ admissible values of $\partial\sigma/\partial f$ at $f = 0$ are the eigenvalues of the matrix

$$\frac{1}{2}\begin{pmatrix} 0 & \mathbf{a} \\ \mathbf{a}^T & 0 \end{pmatrix}$$

where $\mathbf{a} \equiv \|a_{nn'}\|$. The index n ranges over r, s, t, ... and n' over r', s', t', ... Moreover, $|N-N'|$ of these eigenvalues are zero, and the remainder occur in pairs with opposite sign and equal magnitude.

PART 3. CONCLUSION

11. Summary and conclusions

Detailed numerical calculations were made for the frequencies and modal structures of the free gravitational oscillations in rotating rectangular basins of uniform depth, under the quasistatic and planar approximations. The free oscillations consist of antisymmetric and symmetric modes as noted by Taylor (1922). In each family, there are modes propagating in the positive and negative directions of the basin. In general, the antisymmetric modes consist of an odd number of wave systems and the symmetric modes an even number.

The classical result of Taylor (1922) for the slowest positive antisymmetric mode in a 2×1 rectangle rotating with an angular speed equal to the slowest zero-rotation oscillation was verified. Good agreement was also obtained with the frequency values given by Corkan & Doodson (1952) for the slowest positive and negative antisymmetric modes in a square basin. The analytic result of Van Dantzig & Lauwerier (1960) for the frequency of the slowest positive and negative antisymmetric modes in a square basin was found to give good results up to rotation values of $2\omega/\nu_1 \approx 0{\cdot}75$ for the positive mode and $2\omega/\nu_1 \approx 0{\cdot}6$ for the negative.

The calculations show the frequency-splitting of certain multiplets in the zero-rotation spectrum. Also the curves of modal frequency as a function of rotation for some of the modes exhibit a surprising reversal in the sign of the slope; a property that is not exhibited, for example, in the case of a circular cylinder. Further, in the square or rectangular geometry, in the spectrum of modes

associated with a fixed longitudinal or transverse wave-number there can be more than one gravitational mode for which $\sigma < f$.

As far as the structural characteristics of the modes are concerned, it is possible to say the following: rotation of any given rectangle transforms the slowest zero-rotation antisymmetric mode into a positive wave. The corresponding transverse mode is transformed into a negative wave for slow rotations, but continuously changes its structure into a set of positive waves as rotation increases, as was originally found by Corkan & Doodson (1952) in a square basin. The slowest zero-rotation symmetric mode is transformed, on introduction of rotation, into two positive waves. The slowest negative symmetric mode consists of two negative waves at small values of rotation. This mode also changes its structure with increasing rotation. The structures of the higher modes are very complicated even at small rotations and do not permit generalization in any obvious manner, except that all negative waves are 'unstable' in the sense noted above.

An analysis of the spectral dynamic equations in the limit of $f \to 0$ showed that there is a class of modes for which the planar approximation is not valid. These are the modes for which the rotation-induced frequency shift from the zero-rotation value is of $O(f^2)$. The classical frequency results for the case of no redundancy or one redundancy in the zero-rotation frequency spectrum are extended to include an arbitrary number of redundancies.

It was demonstrated that for highly elongated basins one can ignore the effect of the earth's rotation on the period of the lowest longitudinal oscillation and adequately take these effects into account through a Kelvin-wave approximation.

Experimental work was carried out to determine the frequencies of the slowest positive and negative antisymmetric modes and the slowest positive symmetric mode, for various rotation speeds. Quantitative agreement of the experimental and theoretical values of the ratio of frequency to the zero-rotation value was found to be good. The importance of the effects due to free-surface curvature for some of the modes is brought out through a suitable use of the experimental results and theoretical results under the planar approximation.

It is a pleasure to extend my grateful thanks to Prof. George W. Platzman for his constant help and guidance in the course of this work and for his patient and critical review of the manuscript. I also gratefully acknowledge the facilities and assistance given by Prof. Dave Fultz in the experimental work, which was performed in his laboratory.

I have derived much benefit from various discussions with my colleagues Dr M. Miyazaki, T. S. Murty, Thomas W. Flattery and Jack A. C. Kaiser. Judith L. Thieleker and Erik D. McWilliams assisted in certain programming aspects of the problem. Stanley M. Nawrot was most helpful in problems connected with the experimental set-up. Michael Z. Fain and Anthony Kordecki have assisted in the electronic aspects of the experimental set-up, and George W. Gray in the photographic work. I should like to extend my sincere appreciation for all the help I received from these people.

This investigation was supported through funds provided by the National Science Foundation (Grant NSF-GP-471, Technical Report 18, June 1965).

REFERENCES

CORKAN, R. H. & DOODSON, A. T. 1952 Free tidal oscillations in a rotating square sea. *Proc. Roy. Soc.* A, **215**, 147.

DEFANT, A. 1925 *Gezeitenprobleme des Meeres in Landnähe.* (Problem der Kosmischen Physik, 6.) Hamburg: Henri Grand.

DEFANT, A. 1961 *Physical Oceanography*, vol. II. New York: Pergamon Press.

FULTZ, D. 1962 An experimental view of some atmospheric and oceanic behavioral problems. *Trans. N.Y. Acad. Sci.* **24**, 421.

GOLDSBROUGH, G. R. 1931 The tidal oscillations in rectangular basins. *Proc. Roy. Soc.* A, **132**, 689.

JEFFREYS, H. 1925 The free oscillations of water in an elliptical lake. *Proc. Lond. Math. Soc.* **23**, 455.

LAMB, H. 1924 *Hydrodynamics*, 5th ed. Cambridge University Press.

LAMB, H. 1932 *Hydrodynamics*, 6th ed. Cambridge University Press.

MILES, J. W. 1964 Free-surface oscillations in a slowly rotating liquid. *J. Fluid Mech.* **18**, 187.

PLATZMAN, G. W. & RAO, D. B. 1964 The free oscillations of Lake Erie. *Studies on Oceanography* (Hidaka volume) (K. Yoshida, editor), pp. 359–382. University of Washington Press.

PROUDMAN, J. 1916 On the dynamical theory of tides. Part II. Flat seas. *Proc. Lond. Math. Soc.* (2nd Series), **18**, 21.

PROUDMAN, J. 1933 Note on the free tidal oscillations of a sea with slow rotation. *Proc. Lond. Math. Soc.* (2nd series), **35**, 75.

PROUDMAN, J. 1953 *Dynamical Oceanography.* London: Methuen.

RAO, D. B. 1965 Free gravitational oscillations in rotating rectangular basins. Ph.D. Thesis, Department of the Geophysical Sciences, The University of Chicago.

RAYLEIGH, LORD 1903 On the vibrations of a rectangular sheet of rotating liquid. *Phil. Mag.* **5**, 297.

RAYLEIGH, LORD 1909 Notes concerning tidal oscillations upon a rotating globe. *Proc. Roy. Soc.* A, **82**, 448.

TAYLOR, G. I. 1922 Tidal oscillations in gulfs and rectangular basins. *Proc. Lond. Math. Soc.* **20**, 148.

VAN DANTZIG, D. & LAUWERIER, H. A. 1960 The North Sea Problem. IV. Free oscillations of a rotating rectangular sea. *Proc. K. ned. Akad. Wet.* (Series A), **63**, 339.

VELTKAMP, G. W. 1960 Spectral properties of Hilbert Space operators associated with tidal motions. Ph.D. Thesis, University of Utrecht.